Article

Fabrication, Characterization, and Microbial Biodegradation of Transparent Nanodehydrated-Bioplastic (NDBs) Membranes (NDBs) Using Novel Casting, Dehydration, and Peeling Techniques

Sherif S. Hindi [1,*] and Mona Othman I. Albureikan [2]

[1] Department of Agriculture, Faculty of Environmental Sciences, King Abdulaziz University (KAU), P.O. Box 80208, Jeddah 21589, Saudi Arabia
[2] Department of Biological Sciences, Faculty of Science, King Abdulaziz University (KAU), P.O. Box 80208, Jeddah 21589, Saudi Arabia; malboraikan@kau.edu.sa
* Correspondence: shindi@kau.edu.sa

Abstract: NDBs were fabricated from gum arabic (GA) and polyvinyl alcohol (PVA) in different ratios using novel techniques (casting, dehydration, and peeling). The GA/PVA blends were cast with a novel vibration-free horizontal flow (VFHF) technique, producing membranes free of air bubble defects with a homogenous texture, smooth surface, and constant thickness. The casting process was achieved on a self-electrostatic template (SET) made of poly-(methyl methacrylate), which made peeling the final product membranes easy due to its non-stick behavior. After settling of the cast membranous blind, sheets were dried using nanometric dehydration under a mild vacuum stream using a novel stratified nanodehydrator (SND) loaded with P_2O_5. After drying the TBM, the dry, smooth membranes were peeled easily without scratching defects. The physicochemical properties of the NDBs were investigated using FTIR, XRD, TGA, DTA, and AFM to ensure that the novel techniques did not distort the product quality. The NDBs retained their virgin characteristics, namely, their chemical functional groups (FTIR results), crystallinity index (XRD data), thermal stability (TGA and DTA), and ultrastructural features (surface roughness and permeability), as well as their microbial biodegradation ability. Comparing the two TBM' s precursors, PVA had a higher crystallinity index (CI), more mass loss at higher temperatures, greater thermal stability due to higher heat resistance, and a higher clearance of surface roughness due to its large particle size (PS), as well as its higher permeability parameters, namely pore diameter (PD) and void volume (VV), than those for GA. Accordingly, increasing the PVA allocation in the bioplastic blends can enhance their properties except for mass loss, whereby increasing the GA allocation in the TBM blend reduces its mass loss at an elevated temperature. In addition, there is no statistical difference between the NDBs and ordinary air-dried NDBs in PS, PD, and VV, indicating that the novel procedures used did not distort their parent properties examined, as well as their ability for biodegradation. In comparison to control samples, the separated bacteria and fungus destroyed the NDBs. *Pseudomonas* spp. and *Bacillus* spp. were the two main strains of isolated bacteria, and *Rhizobus* spp. was the main fungus. The nanodehydration method gave the best solution for the prompt drying of water-based biopolymers free of manufacturing defects, with simple and easily acquired machinery required for the casting and peeling tasks, in addition to its wonderful biodegradation behavior when buried in wetted soil.

Keywords: bioplastic; gum arabic; polyvinyl alcohol; dehydration; FTIR; XRD; TGA; DTA; AFM; microbial biodegradation

1. Introduction

Despite petroleum-based polymers' lower density and greater mechanical characteristics, biobased polymers have gained significant interest due to growing environmental

Preprints (www.preprints.org) | NOT PEER-REVIEWED | Posted: 25 May 2023 doi:10.20944/preprints202305.1803.v1

concerns about their sustainability and biodegradability [1–6]. Many biopolymers, including poly-lactic acid/poly-lactide, poly-3-hydroxy-butyrate, starch, gelatin, alginate, agar agar, guar gum, and GA, have been used in various industrial applications.

GA is a type of edible natural exudate gum arising from the mature trunks and branches of various acacia species, especially *Acacia senegal*, *A. seyal*, *A. nilotica*, and *A. mellifera* (family: Fabaceae) [7]. The GA yield can be enhanced by drought conditions or poor soil fertility and with injured or scratched plants to cover the huge demand for domestic and industrial applications due to its water-soluble and polysaccharide nature [8–10].

Chemically, GA has hydrophilic carbohydrates (arabinogalactans), as well as hydrophobic proteins (the arabinogalactan-protein complex and glycoproteins) that exhibit various functional properties in food additives [11–15]. It is well-known that D-galactose, l-arabinose, L-rhamnose, D-glucuronic acid, and 4-O-methyl-d-glucuronic acid make up the highly branched complexes known as arabinogalactan-proteins, along with a minor amount of proteins. While hydrophilic arabinogalactan provides steric and electrostatic stability, this hydrophobic polypeptide chain can tie gum to oil droplets in emulsion [15]. The benefit of the amphiphilic nature of GA is in preventing coalescence, which can promote film formation and display steric stabilization. Furthermore, GAs have significant effects on various emulsion factors, including opacity, specific gravity, zeta potential, and surface tension [15].

GA is used primarily in the food, medicinal pharmaceutical, and wood technology industries [15–33] as a stabilizer, emulsifier, and thickening agent [15–18], because of its high hydrophilicity, low fluidic viscosity, good surficial activities, and ability to form a protective film around emulsion droplets [15]. Recently, the use of GA has been extended into the nanotechnology and nanomedicine fields due to its biocompatibility for both in vivo and in vitro applications and its stabilization of nanostructures. GA has been probed for its coating properties and increased biocompatibility of iron oxide magnetic nanoparticles [34,35], gold nanoparticles [36], carbon nanotubes [37], and quantum dot nanocolloids [38].

PVA is a synthetic polymer with a wide range of commercial applications due to its high crystallinity, good mechanical properties, water solubility, and adhesive properties [39–42]. These applications extend to the industrial, medical, pharmaceutical, and food sectors and include lacquers, resins, surgical threads, food packaging materials [26,29,40], paper coating, textile sizing [43], and for coating purposes [44], where it is used in order to enhance the mechanical properties due to natural properties, such as compatible structure and hydrophilic properties [45]. Furthermore, it is used as a thermoplastic polymer for living tissues because it is harmless and non-toxic, as well as functioning as a cross-linker and nanofiller [46–48]. Furthermore, since PVA has excellent chemical resistance, it is used as a good emulsifier [49].

Practically, PVA is widely blended with other hydrophilic polymers [45], such as GA, to enhance its mechanical properties as well as its biodegradability [42,50–56]. However, the drawbacks that are associated with the manufacturing of bioplastic materials are the drying process for the cast GA membrane due to the high water content of the parent material, thereby making the entire process time- and cost-intensive. Hence, there exists a need to develop an apparatus or method which overcomes the above limitations [57]. The presence of a large number of hydroxyl, carboxylic, and carbonyl groups in the GA/PVA blends makes it a chemical reductant and environmentally benign medium [58]. PVA is easily degradable by biological organisms [39,58], and many microorganisms that are able to degrade PVA and GA have been identified [59–62].

Different GA composites were prepared and characterized by several researchers for fabricating films and membranes [63–65], as well as for anodes of lithium-ion batteries [66]. In addition, Silvestri et al. [67] produced nanofibers from a blend containing GA (10 wt% solution), graphene oxide (GO), and PVA, while Lubambo et al. [68] obtained nanofibers from guar gum.

 doi:10.20944/preprints202305.1803.v1

The processing of GA includes impurity removal, kibbling, granulating, grinding, powdering, acid or enzymatic hydrolysis, clarification and discoloration, centrifugation (10,000–16,000 rpm/min), purification of the ceramic membrane, desalination, and spray drying [69–73].

A particular category of polymers known as biodegradable polymers [74–88] degrade naturally into byproducts such as gases (CO_2 and N_2), water, biomass, and inorganic salts [57] after serving their intended purpose. The abiotic and biotic components of the biodegradation mechanism coexist in the soil naturally [2,6]. Recently, a lot of biodegradable polymers have been created, and some known microbial enzymes can break them down [5]. Numerous microbial communities of bacteria, fungi, and yeasts, including but not limited to Gram-negative species, such as *Escherichia coli* and *Pseudomonas aeruginosa*, and Gram-positive species, such as *Staphylococcus aureus*, can use bioplastic as a nutrition source throughout the biodegradation process [1,3,4,55]. These include *Rhizobium meliloti* [5], *Bacillus* spp. [58], *Pseudomonas* spp., *Aspergillus* spp., *Rhizorpous* spp., *Fusarium* spp., *Penicillium* spp., *Saccharomyces* as yeast [59], and *Elite Aspergillus* [86]. Under aerobic (composting) or anaerobic (landfill) conditions, several petroleum-based polymers are biologically decomposable [47,89].

By combining synthetic and natural polymers, researchers have been able to improve the processing capacity, physicochemical characteristics, and biodegradability of synthetic polymers [1,4,6,50–53]. For various polymers, including PVA, the rates and environmental factors that influence breakdown might vary [47,60,90–92]. Composting can take place under different conditions, including in anaerobic environments, underground soil layers, aqueous media, and even in the presence of oxygen.

The aims of the present work were: (a) to invent a more reliable bioplastic membrane that is suitable for different applications, (b) to overcome the casting, drying, and peeling problems of the hydrophilic bioplastic (GA/PVA) blends, (c) to compare the ordinary GA/PVA bioplastic membranes (ADBs) with those synthesized using the novel methods in the present investigation (NDBs), and (d) to study the biodegradation behaviors of the NDBs when buried in wetted soil.

2. Materials and Methods

The management plan for the production of novel transparent NDBs is illustrated in Figure S1.

2.1. Raw Material

GA (~ Mw: 1.827 × 106 g/mole) was harvested from the trunks and branches of Acacia seyal trees (Figure 1a1) habituated at Hada Al-Sham (about 120 km apart from Jeddah), Saudi Arabia. GA was collected from tree sap exuded out of the trunks and/or branches of the tree after tapping the woody tissues of the tree and making incisions (60 cm × 5 cm).

Preprints (www.preprints.org) | NOT PEER-REVIEWED | Posted: 25 May 2023 doi:10.20944/preprints202305.1803.v1

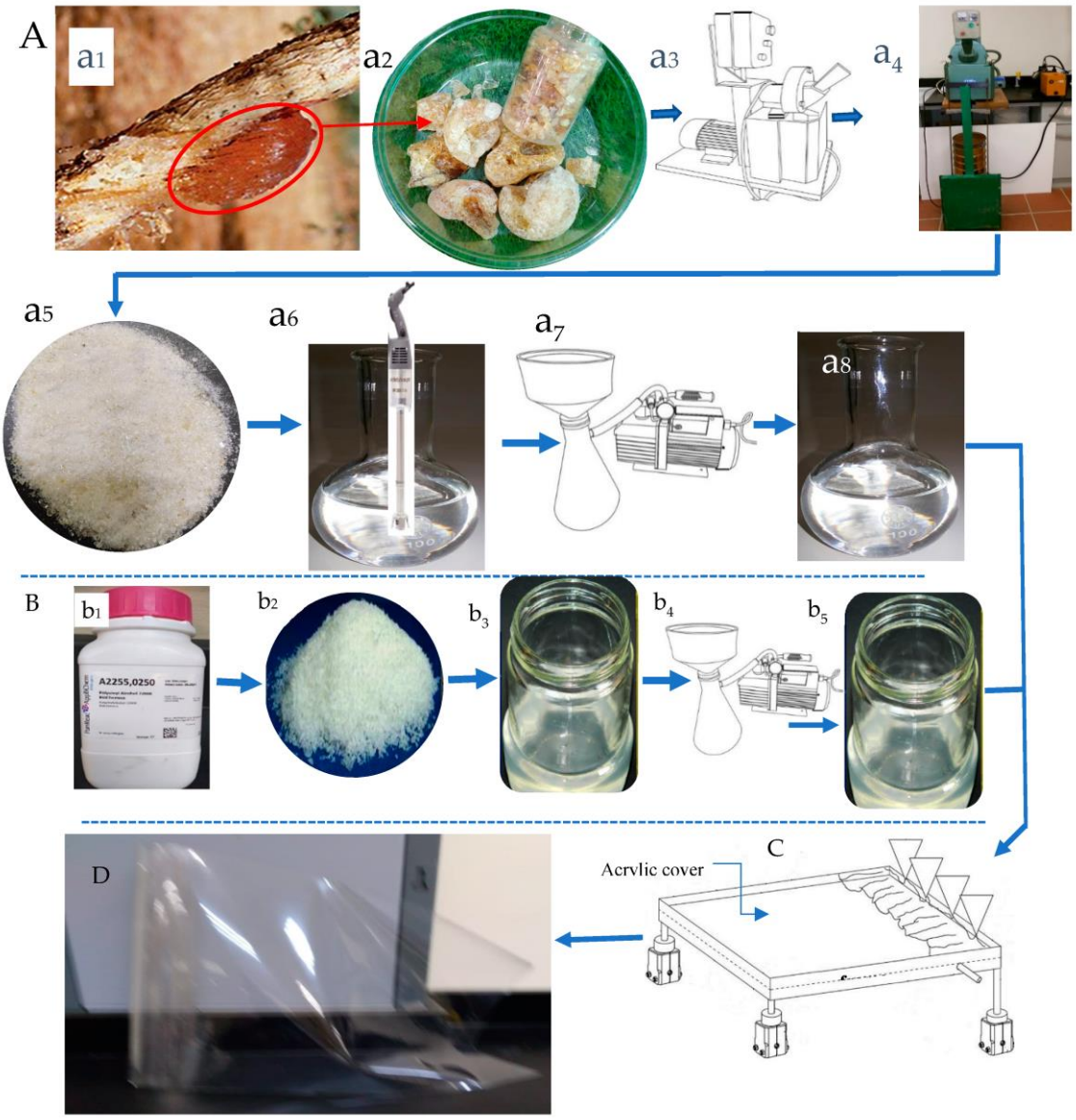

Figure 1. Manufacturing of NDBs: (**A**) Harvesting and processing of the GA principle precursor: (**a**$_1$) hardened sap naturally excreted on a branch of an *Acacia seyal* tree; (**a**$_2$) crude GA granules; (**a**$_3$) mechanical grinder; (**a**$_4$) vacuum-assisted sieving system; (**a**$_5$) uniform powder of crude GA; (**a**$_6$) crude solution of well-dissolved GA; (**a**$_7$) vacuum-filtration device; (**a**$_8$) clear vacuum-filtered solution. (**B**) PVA-modifier precursor: (**b**$_1$) analytical-grade bottle; (**b**$_2$) powder form; (**b**$_3$) crude solution of well-dissolved PVA; (**b**$_4$) vacuum-filtration device; (**a**$_5$) clear vacuum-filtered solution; (**C**) VFHF device; (**D**) the TBM final produt.

2.2. Preparation of the Chemical Reagents

2.2.1. GA

As shown in Figure 1A, the naturally hardened sap excreted on a branch of an *Acacia seyal* tree was collected (Figure 1a$_1$) and cured into crude granules (Figure 1a$_2$). The solid granules were ground using a mechanical grinding machine (Figure 1a$_3$), passed through a standard 60 mesh sieve, and retained particles of 80 mesh size (60/80 mesh) using a vacuum-assisted sieving system (Figure 1a$_4$). About 50 g of air-dried uniform GA powder (Figure 1a$_5$) was dissolved in one liter of deionized water at ambient temperature (25 °C) and heated up to 80 °C with continuous stirring until all particles were completely dissolved (Figure 1a$_6$). Removing the insoluble components of the resultant solution was achieved via vacuum filtration (Figure 1b$_7$) to obtain the clear GA precursor at a concentration of 5%, wt/wt (Figure 1a$_8$).

 doi:10.20944/preprints202305.1803.v1

2.2.2. PVA

PVA was used as a modifier precursor to synthesize the TBM, along with GA. PVA used in this investigation (Figure 1B) was of ACS reagent quality (Figure 1b$_1$), Mw 88,000 Da, and 88% deacetylated. About 50 g of PVA crystals (Figure 1b$_2$) were dissolved in one liter of deionized water to obtain a crude solution (Figure 1b$_3$) as a result of heating under continuous stirring at 80 °C until complete clearance and subsequently, vacuum-filtered (Figure 1b$_4$) to obtain the clear PVA precursor at a concentration of 5%, wt/wt (Figure 1b$_7$).

2.3. Preparation of the Bioplastic Blends

The practical procedure used for the novel casting of the bioplastic blends is presented in Figure S2. Six different bioplastic blends of GA and PVA in different ratios were prepared by mixing their aqueous solutions (5% wt/wt each) under continuous calm stirring until the solution became completely homogenous (see Figure 1). It is crucial to stir slowly and carefully to prevent the addition of too many air bubbles to the solution, which can result in aeration defects in the final membranous product.

2.4. Casting the Bioplastic Blends

After obtaining complete homogeneity for the biopolymer blend, the bubble-free ternary blend solution was poured onto a clean acrylic panel. This panel is the surficial layer of the VFHF device (Figures 1C and S3), with a prominent frame where it is necessary to adjust the initial thickness of the bioplastic membrane to determine its final thickness. After that, the cast blend was allowed to dry at ambient temperature using the novel stratified nanodehydrator (SND) apparatus [57,93,94], as shown in Figure 2.

Preprints (www.preprints.org) | NOT PEER-REVIEWED | Posted: 25 May 2023 doi:10.20944/preprints202305.1803.v1

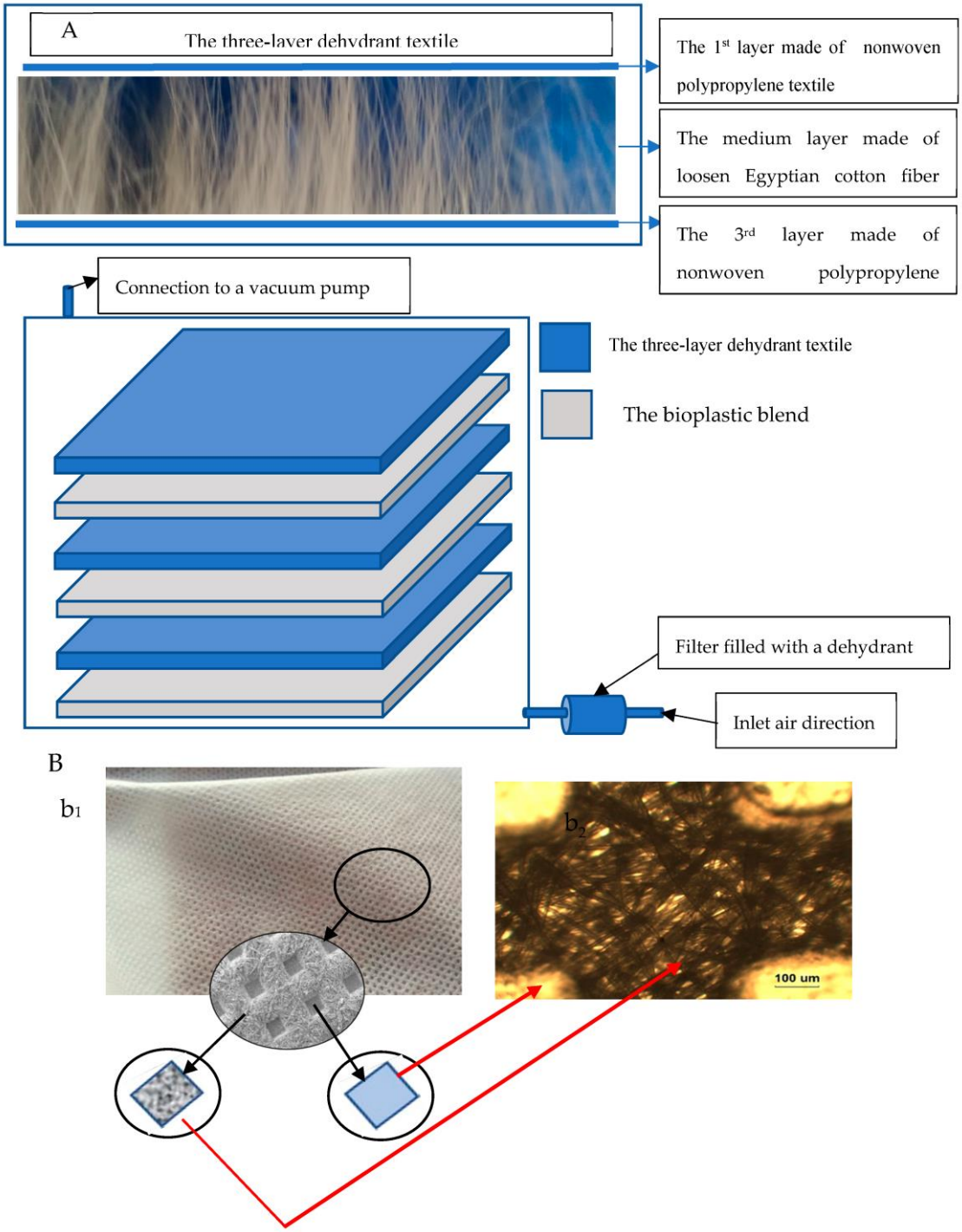

Figure 2. The novel nanodehydration technique: (**A**) the stratified air-dryer apparatus, and (**B**) the non-woven textile of polypropylene: (**b1**) an optical image, and (**b2**) microscope image (40X) according to Hindi and Albureikan [57].

The novel VFHF device (Figures 1C and S3) features both the ease of casting the blend and peeling the membranes with a constant thickness free of air bubbles. For manufacturing a TBM, the blend was poured after adjusting the slope angle of the acrylic ground template (Figures 1C and S3) to a slight angle (about 15°) to accelerate the blended fluid movement. The slow motion of the blend protects its matrix from forcing more bubbles inside it. After the blend reached the opposite side of the template, the slope angle was re-adjusted to zero degrees to ensure exact horizontality in order to obtain identical thicknesses. It is worth mentioning that the thickness of the bioplastic sheets was controlled by

Preprints (www.preprints.org) | NOT PEER-REVIEWED | Posted: 25 May 2023 doi:10.20944/preprints202305.1803.v1

two critical actions: (a) pouring a definite quantity of blend solution onto the same template area and (b) accurate adjustment for the viscosities of these blends [57].

In order to obtain gentle, steady, and efficient flow for the viscous bioplastic blend, each of the four legs of the VFHF was fixed with a vibrating magnetic solenoid (a Kendrion OSR series shaker solenoid) designed with two excitation coils to generate a harmonious vibrating movement in the blend [57]. The magnetic vibrating system (Figure S3B) consists of a permanent magnet at the bottom, connecting the magnetic body's two halves and two excitation windings. The body to be vibrated, which serves as the armature, closes the magnetic circle through an air gap. A steady pulling force between the magnetic body and armature is produced by the permanent magnet that is integrated into the magnetic body, biasing the system. The alternating electromagnetic field's force effect superimposes itself onto the permanent magnet's force effect when an AC voltage is delivered to the excitation coil. The fully encapsulated bobbin and coils achieve reliable long-life service and maintenance-free operation. In addition, OSR shaker solenoids are not susceptible to dust or moisture when operational under rough or adverse conditions [57]. It is worth mentioning that a permanent magnetic attachment serves to mount the OSR shaker solenoid freely and that it is detachable from the vibrating surface. Angle mounts permanently fix the OSR shaker solenoid to a vibrating surface. In addition, phase angle controllers were installed separately for the fine adjustment of vibration through an alternating or direct current (via an integrated one-way rectifier), and they can be DIN-rail mounted within cabinets with minimal space.

2.5. Drying the NDBs

The Stratified Nano-Dehydrator (SND)

The most critical problem concerning the manufacturing of bioplastic sheets is their drying process, where it is crucial to obtain high-quality products. This problem arises from the highly hydrophilic nature of bioplastic sheets blended from mixtures of hydrophilic GA and PVA in different ratios.

The SND was invented to accelerate the dehydration process of bioplastic sheets [57]. As shown in Figure 2, it consists of three stratified and perforated acrylic panels (polymethyl methacrylate). These panels were arranged in a vertically alternating pattern, with three sub-layers consisting of dehydrant-loaded fibrous materials. Each sub-layer constitutes two non-woven polypropylene textiles, restricting an intermediate net of loosened Egyptian cotton floss (ECF). All fibrous materials constructing the sub-layer are saturated with a strong dehydrant, such as phosphorus pentoxide (P_4O_{10}), the most highly preferred dehydrant reagent, rather than calcium chloride or silica gel. This cellulosic material was selected for this task due to its high content of alpha cellulose, well-known for its high hydrophilicity, which is essential to attain good affinity to both moisture molecules, as well as dehydrant crystals. The manner of loading dehydrant onto the cellulosic fibers can be summarized as follows: (1) air-drying of cellulosic fibers used as a core skeleton of the SND; (2) preparing dehydrant saturated solution; (3) soaking cellulosic fibers in the salt-saturated solution via vacuum forces to ensure complete immersion and saturation of the fiber cells, and penetration of the salt solution into the cell cavities, as well as the cell wall, through the internal border pits of the cellulosic fibers; (4) discarding of excess salt solution, and drying the cellulosic fibers by air-drying and finally oven-drying at 80 °C ± 5°C for 2 h; (5) this medium layer was inserted between the first and third layers, which were made of non-woven polypropylene textile. The edges of the outer layers were welded thermally due to the nature of polypropylene as a thermoplastic material. Furthermore, the three-layer textile was reinforced upon stitching using a sewing machine.

 doi:10.20944/preprints202305.1803.v1

2.6. Characterization of the Bioplastic Membranes

2.6.1. FTIR

Using a Bruker Tensor 37 FTIR spectrophotometer, the chemical constituents and functional groups of the six bioplastic membranous samples were investigated. The samples were combined with KBr at a ratio of 1:200 wt/wt and compressed under vacuum to form pellets after being oven-dried at 100 °C for 4–5 h. The materials' FTIR spectra were captured between 400 and 500 cm^{-1} in transmittance mode.

2.6.2. X-ray Diffraction (XRD)

An XRD 7000 Shimadzu diffractometer (Japan) was used to determine the XRD spectra of the six bioplastic sheets. An anode generator, a copper target, and a wide-angle powder goniometer are all parts of the system. Measurements were performed with the aid of CuK radiation arising at 30 kV and 30 mA. The Kα1 (0.15406 nm) and Kα2 (0.15444 nm) components of the CuK radiation are present in the resulting XRD data.

A single-channel analyzer was used to extract data resulting from the semiconductor detector. The reception slit was 0.15 mm at the same radius, and the divergence and scatter slits were each 10 m wide. Several droplets of diluted amorphous glue were used to mount dried bioplastic sheets (weighing around 0.5 g) onto a quartz substrate. Each sample was scanned in the 2 θ° range between 5° and 40°. Every experiment was run in reflection mode, with increments of 0.05° and a scan speed of 4°/min [57,93].

The crystallinity index (CI) was computed by dividing the diffractogram area of crystalline cellulose by the entire area of the original diffractogram after smoothing the resulting crystalline peaks from the diffraction intensity profiles. Using Microsoft Excel (USA), the area under the curve was calculated by adding adjacent trapezoids [93–97,98].

2.6.3. Thermal Analysis

Since DTA typically complements TGA with information on phase transitions [93], the TGA and DTA of each blend were conducted simultaneously. These characterizations were carried out for TGA and DTA for all six bioplastic blends [57,93,94,96] using a Seiko & Star 6300 analyzer, Central Laboratory, Faculty of Science, Alexandria University, Egypt.

Using a heating rate of 20 °C/min under a nitrogen atmosphere, heating scans were carried out from 30 °C up to the final maximum temperature of 450 °C [57,93,96].

The following equation was used to determine TBM mass loss from the TGA curves shown in Figure 5: Mass loss = $[(W_2 - W_1)/W_1] \times 100$, where W_1 is the initial TBM weight for this temperature zone, W_2 is the final TBM weight for the same temperature zone, and the mass loss as a percentage was obtained.

2.6.4. Surface Topography (ST) [57,93]

Atomic force microscopy (AFM) was used to examine the surfaces of the six NDBs in order to observe the full 3D membranous surface structures down to the nanometric scale. Four distinct characteristics of the TBM were revealed by AFM: surface roughness (SR), nanometric particle size (NPS), pore diameter (PD), and void volume (VV).

2.7. Microbial *Biodegradation*

Microbial biodegradation was assessed to investigate the microbes' capacity to break down the buildup of bioplastic in soil. Upon calculating the percentage of biodegradation (weight loss), counting the microbe population isolated from the surfaces of bioplastic sheets, and evaluating the various morphological changes in these surfaces as a result of degradation, it was possible to determine the amount of biodegradation [93,94].

The soil was collected from the Agricultural Research Station (ARS) of King Abdullaziz University's Faculty of Environment Sciences in Hada Al-Sham and was used to bury the bioplastic samples. The location is situated 240 m above sea level, around 120 km

 doi:10.20944/preprints202305.1803.v1

to the northwest of Jeddah (N= 21° 48- 3=, E= 39° 43 25). The pH of the soil at the site ranged from 7.1 to 7.9, along with low levels of $CaCO_3$, organic matter, and cation exchange capability [99,100].

2.7.1. Sample Preparation and Soil Burial Studies

The various bioplastic sheets were shredded into 2 cm × 2 cm pieces and buried 10 cm deep in 100 g wet soil boxes. Before being buried in the ground, each bioplastic piece was weighed (0.040–0.038 g). By adding sterile water to the soil samples to counteract water evaporation, the moisture content of the soil samples was kept constant [93].

Each sample box had a hole at the bottom for the excess water to drain through. After 30 and 60 days, soil samples were carefully removed, and the weight loss was calculated in order to separate, count, and compare the microbial community, as well as speculate on microbial morphology changes as a result of degradation [93,94,101].

2.7.2. Isolation and Counting of Microbial Communities

About 95 mL of sodium pyrophosphate solution at 0.1% wt/v was used to suspend one gram of soil collected from the surface of the bioplastic sheets from each sample. The samples were left to stand for 30 min. Then, using the serial dilution method, the supernatant was divided among six tubes, and one milliliter (mL) of each dilution was plated on nutrient agar medium NA (Oxoid) for the isolation of bacteria, while potato dextrose agar medium PDA (Oxoid) was used for the isolation of fungi.

Finally, in order to determine the colony-forming units (CFU), plates were incubated at 30 °C and pH 7 for 72 h (for bacteria) and at 25 °C and pH 5 for 24 h (for fungi). Based on the cultural and physical characteristics, microorganisms were separated and identified using conventional assays [1,57,93,94].

2.8. *Statistical Design and Analysis*

Various properties of the six bioplastic membranes synthesized from the aqueous solutions of GA and PVA were assessed using a randomized complete block design. According to El-Nakhlawy [102], a statistical analysis of the obtained data was carried out using the analysis of variance approach and the least significant difference test (LSD) at 0.05.

3. Results

3.1. Chemical and Physical Properties of the Bioplastic Membranes

3.1.1. FTIR

FTIR spectroscopy was used to determine the chemical functionality of the bioplastic sheets (the nanodehydrated membranes (NDMs), as illustrated in Figure 3. The spectra of the resulting NDBs exhibited chemical group absorption bands that were typical of the gummy products made from both GA and PVA in different ratios. The absorption bands spanned an area between 500 and 4000 cm^{-1}. Several chemical groups were precisely found at the following wavenumbers: 900–1250, 1426, 1402, 1625.4, 1627.4, 1430, 1436.91, 1437, 1641, 1047, 2800–3000, 2885, 2910.87, 2939, 3000, 3261, 3416, 3000, and 3600 cm^{-1} [57,93,94,96,103–106].

Preprints (www.preprints.org) | NOT PEER-REVIEWED | Posted: 25 May 2023 doi:10.20944/preprints202305.1803.v1

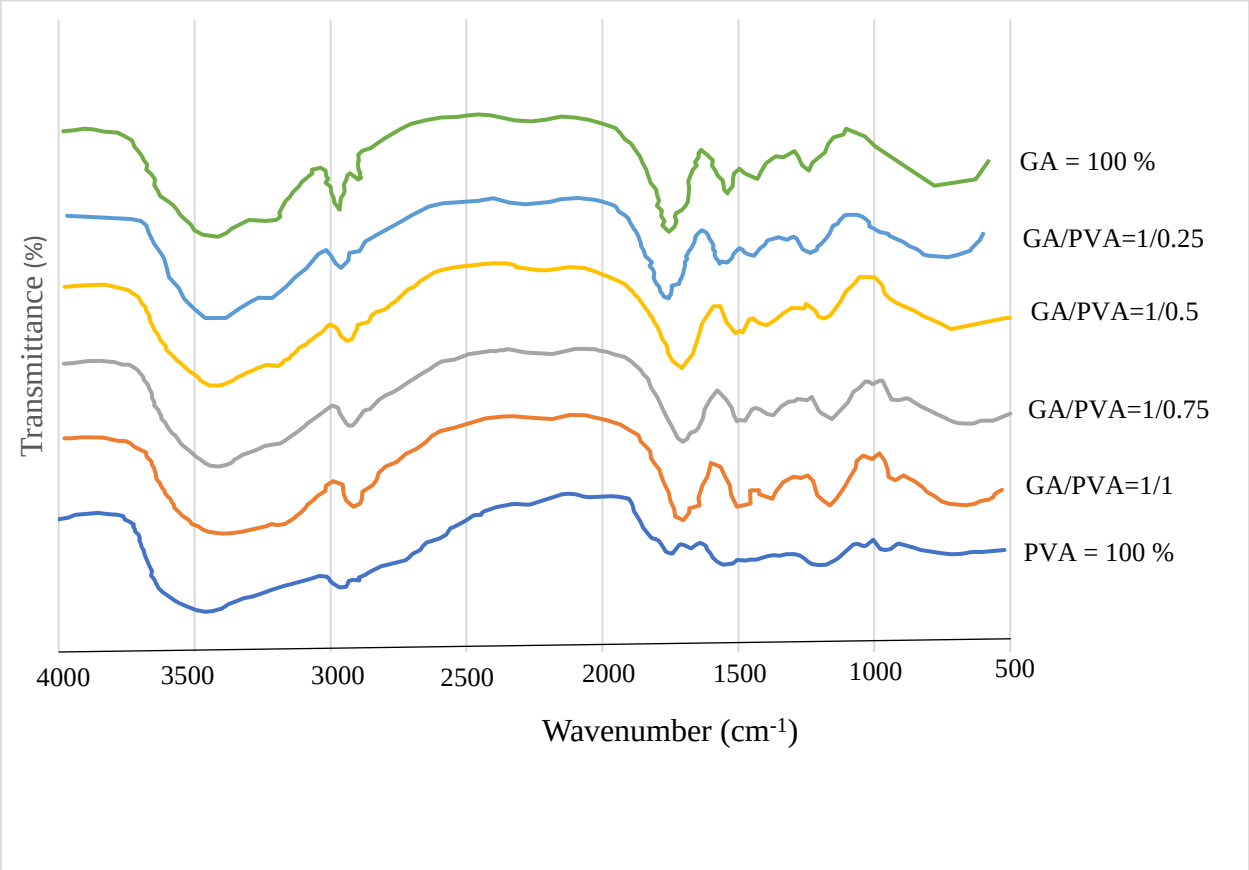

Figure 3. FTIR spectra of the six transparent nano-dehydrated bioplastic membranes (NDBs) over the wavenumber range of 4000 to 500 cm^{-1}, fabricated from various gum arabic (GA)/polyvinyl alcohol (PVA) blends.

3.1.2. XRD

Figure 4 displays the XRD patterns of the six bioplastic membranes. The maximum intensity of the GA-broad diffractogram was obtained at 2Θ = 20°, which confirms the amorphous nature of the gum arabic [13]. Moreover, a typical peak for pure PVA, a semi-crystalline polymer, was visible at 2Θ = 19.9°. With the increase in PVA allocation in the blend, the crystallinity index values increased (Figure 4).

Preprints (www.preprints.org) | NOT PEER-REVIEWED | Posted: 25 May 2023 doi:10.20944/preprints202305.1803.v1

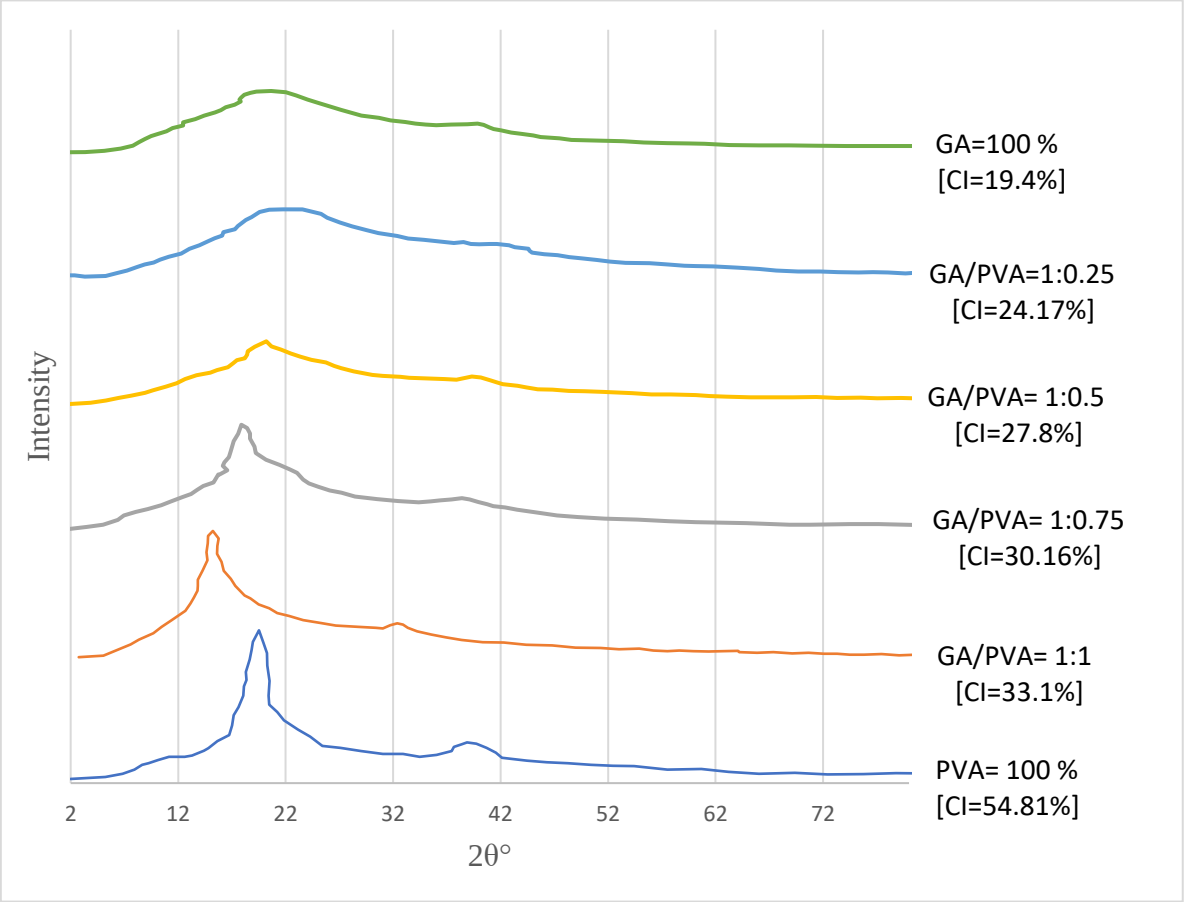

Figure 4. XRD diffractogram spectra of the six transparent nano-dehydrated bioplastic membranes (NDBs) over a wavenumber range of 4000 to 500 cm^{-1}, fabricated from various gum arabic (GA)/polyvinyl alcohol (PVA) blends, showing the crystallinity index (CI) values.

As demonstrated in Figure 4, the CI values of the NDBs were found to increase from 19.4% (for pure GA) to 54.81% (for pure PVA), as shown in Figure 4. Accordingly, it is clear that the increase in CI of the bioplastic blends can be attributed to an increase in the PVA allocation in the blend.

3.1.3. TGA

The TGA results are presented in Figure 5 and in Tables 1 and S6. The mass losses of the six NDBS samples were focused on eight temperature regions, namely 50–100 °C, 100–150 °C, 150–200 °C, 200–250 °C, 250–300 °C, 300–350 °C, 350–400 °C, and 400–450 °C (Tables 1 and S6; Figure 5).

The thermal degradation of the samples increased with rising temperatures for all six bioplastic blends, according to a comparison of mass losses between temperature zones (at the same bioplastic blend ratio).

Comparing the mass losses within the temperature zone meant studying the differences between bioplastic blend ratios in the same temperature zone. It is clear from Tables 1 and S6 and from Figure 5 that at lower temperatures (≤150 °C), PVA lost more weight (5.69% and 8.98% for 50–100 °C and 100–150 °C zones, respectively) than for GA (13.68% and 11.11%) in the same temperature zones. On the other hand, at higher temperatures, this trend was reversed, whereby PVA lost more weight (79.01% and 58.8% for the 400–500 °C and 450–500 °C zones, respectively) than GA (28.6% and 15.6% for the same zones, respectively).

Preprints (www.preprints.org) | NOT PEER-REVIEWED | Posted: 25 May 2023 doi:10.20944/preprints202305.1803.v1

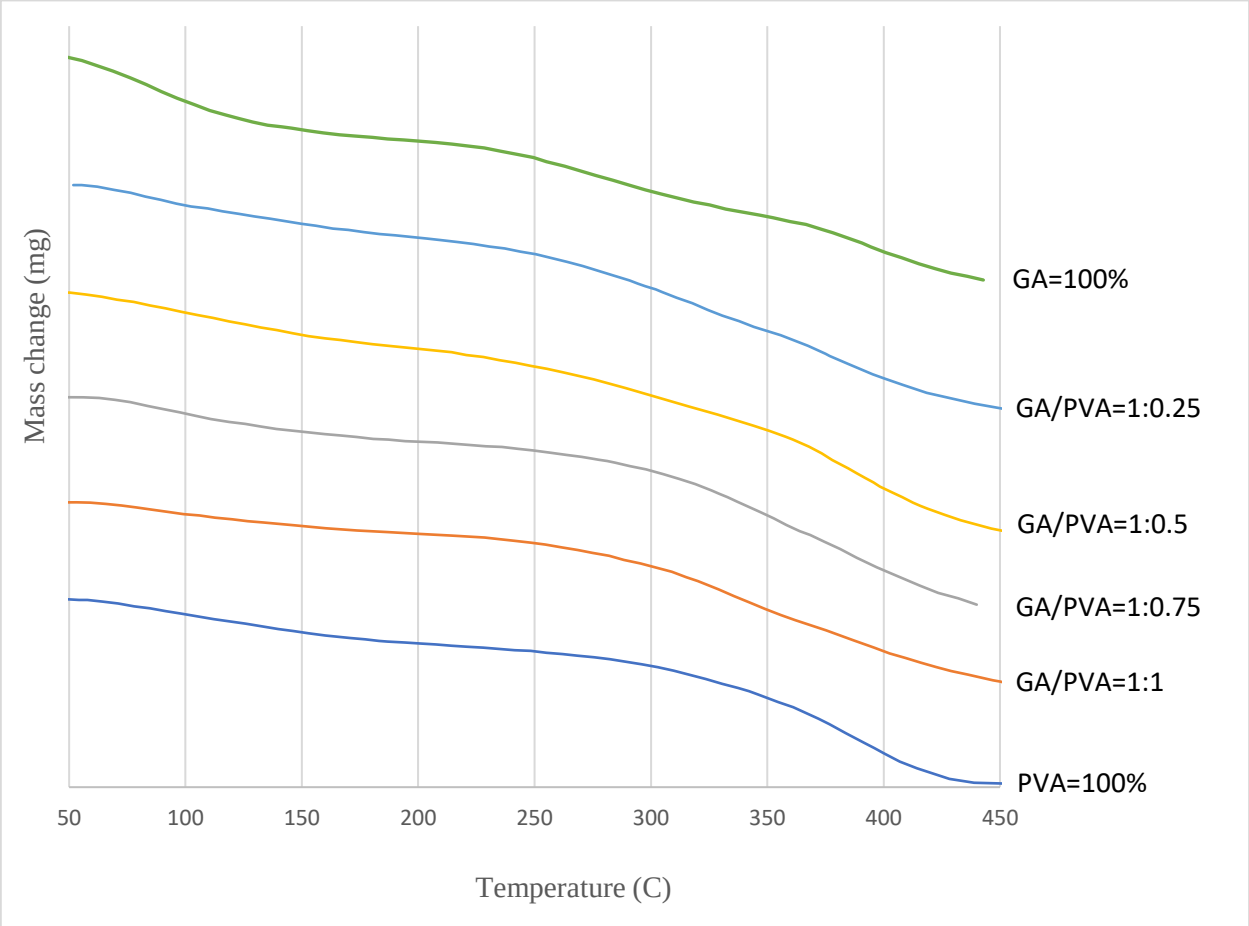

Figure 5. Thermogravimetric analysis (TGA) thermogram spectra of the six bioplastic membranes (NDBs) in the wavenumber range of 4000 to 500 cm^{-1}, fabricated from various gum arabic (GA)/polyvinyl alcohol (PVA) blends.

Table 1. Mean[1–7] values of mass loss (ML) of the six transparent nano-dehydrated bioplastic membranes (NDBs) over a wavenumber range of 4000 to 500 cm^{-1}, fabricated from various gum arabic (GA)/polyvinyl alcohol (PVA) blends over different ratios and temperature (T) zones.

T-Zones ℃	GA/PVA Ratio					
	GA 100%	1:0.25	1:0.5	1:0.75	1:1	PVA 100%
50°–100°	13.68 $^{A}{}_{d}$	4.57 $^{B}{}_{g}$	4.85 $^{B}{}_{e}$	5.02 $^{B}{}_{ef}$	5.23 $^{B}{}_{ef}$	5.69 $^{B}{}_{f}$
100°–150°	11.11 $^{A}{}_{e}$	6.32 $^{AB}{}_{f}$	6.37 $^{AB}{}_{e}$	6.93 $^{AB}{}_{e}$	6.47 $^{AB}{}_{ef}$	8.98 $^{B}{}_{ef}$
150°–200°	4.18 $^{BC}{}_{g}$	4.88 $^{BC}{}_{g}$	6.46 $^{B}{}_{e}$	4.26 $^{BC}{}_{ef}$	3.23 $^{C}{}_{f}$	8.07 $^{A}{}_{ef}$
200°–250°	6.96 $^{B}{}_{f}$	8.18 $^{A}{}_{e}$	6.18 $^{B}{}_{e}$	3.7 $^{C}{}_{f}$	5.71 $^{B}{}_{ef}$	3.9 $^{C}{}_{g}$
250°–300°	7.48 $^{C}{}_{f}$	14.9 $^{A}{}_{d}$	7.36 $^{C}{}_{e}$	10.77 $^{AB}{}_{d}$	11.62 $^{B}{}_{d}$	10.15 $^{AB}{}_{e}$
300°–350°	22.2 $^{B}{}_{b}$	12.62 $^{E}{}_{de}$	15.93 $^{D}{}_{d}$	22.41 $^{B}{}_{c}$	28.57 $^{A}{}_{c}$	18.08 $^{C}{}_{d}$
350°–400°	18.2 $^{E}{}_{b}$	21.13 $^{D}{}_{b}$	26.32 $^{C}{}_{b}$	33.3 $^{B}{}_{b}$	34.4 $^{B}{}_{b}$	44.14 $^{A}{}_{c}$
400°–450°	28.6 $^{D}{}_{a}$	27.68 $^{D}{}_{a}$	41.43 $^{C}{}_{a}$	39.17 $^{BC}{}_{a}$	46.34 $^{B}{}_{a}$	79.01 $^{A}{}_{a}$
450°–500°	15.6 $^{E}{}_{c}$	18.52 $^{D}{}_{c}$	21.95 $^{CD}{}_{c}$	24.66 $^{C}{}_{c}$	45.5 $^{B}{}_{a}$	58.8 $^{A}{}_{b}$

[1] Each value is an average of 3 samples. [2] Based on original oven-dry weight. [3] Superscript capital letters for comparing blend ratios within the same temperature zone. [4] Subscript small letters for comparing temperature zones within the same blend ratio. [5] Means with the same letter are not significantly different at the 5% level. [6] Initial starting weight of the TBM sample. [7] Final starting weight of the TBM sample.

3.1.4. DTA

Preprints (www.preprints.org) | NOT PEER-REVIEWED | Posted: 25 May 2023 doi:10.20944/preprints202305.1803.v1

The DTA analysis findings of the six nanodehydrated transparent nano-dehydrated bioplastic membranes (NDBs) are presented in Figure 6 and Table 2.

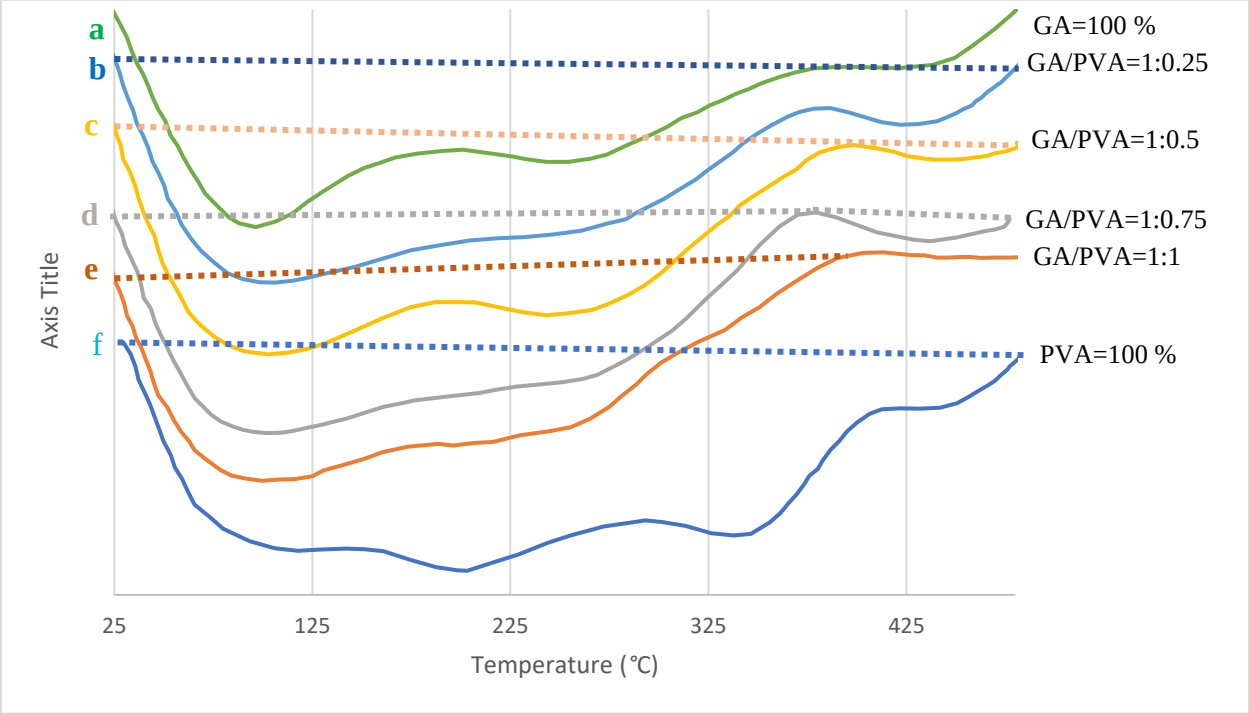

Figure 6. Thermograms of differential thermal analysis (DTA) of the six transparent nano-dehydrated bioplastic membranes (NDBs) over a wavenumber range of 4000 to 500 cm^{-1}, fabricated from various gum arabic (GA)/polyvinyl alcohol (PVA) blends.

Examining Figure 6 and Table 2, the TBM thermograms were found to be divided into two sets representing the bioplastic blends, namely the single-phase and double-phase thermograms. The single-phase thermogram is constituted from one endothermal phase, namely curve 'b' (GA/PVA of 1:0.25), curve 'e' (GA/PVA of 1:1), and curve 'f' (PVA = 100%). On the hand, the double-phase thermogram is differentiated into two distinct regions (endothermic and exothermic), namely curve 'a' (GA = 100%), curve 'c' (GA/PVA of 1:0.5), and curve 'd' (GA/PVA of 1:0.75).

For more information, see Table 2. It is evident from Table 2 that the temperature range of each thermogram and the absolute values of the heat change (HC) values for the endotherms (16 Vs/mg–52.4 Vs/mg) were larger than those for the exotherms. Additionally, among the other bioplastic blends, the pure PVA endotherm absorbed the most energy (2119.7 Vs/mg), but GA had the lowest value of heat change (−1017.3 Vs/mg).

For more information, it is evident from Table 2 that the temperature range of each thermogram and the absolute values of the heat change (HC) values for the endotherms (16 Vs/mg–52.4 Vs/mg) were larger than those for the exotherms. In addition, among the other bioplastic blends, the pure PVA endotherm absorbed the most energy (2119.7 Vs/mg), but GA had the lowest heat change value (−1017.3 Vs/mg).

Preprints (www.preprints.org) | NOT PEER-REVIEWED | Posted: 25 May 2023 doi:10.20944/preprints202305.1803.v1

Table 2. DTA results of the six transparent nano-dehydrated bioplastic membranes (NDBs) in the wavenumber range of 4000 to 500 cm^{-1}, fabricated from various gum arabic (GA)/polyvinyl alcohol (PVA) blends points of reaction, thermogram type, temperature range (TR), and heat change (HC).

	GA/PVA Ratio	Thermogram Type	TR °C	HC µVs/mg
a	GA = 100%	Endotherm	25–265	−1017.25
		Exotherm	265–435	+52.39
b	1:0.25	Endotherm	25–475	−2268.77
c	1.0.5	Endotherm	25–397	−1127.7
		Exotherm	397–480	−16.67
d	1:0.75	Endotherm	25–375	−1276.04
		Exotherm	375–475	−20.89
e	1:1	Endotherm	25–475	−1467.19
f	PVA = 100%	Endotherm	25–475	−2119.72

3.1.5. Ultrastructure of the Bioplastic Membrane

Surface Roughness and Nanometric Particle Size (PS)

In order to confirm the similarity between the ultrastructure features of ADBs and NDBs, surface roughness was investigated via atomic force microscopy (AFM) and is presented in Figure 7 for each of the six bioplastic blends.

The nanometric PS of the bioplastic membranes, the ADEs or NDBs, are presented in Table 3 and Figures 7A–F and 8a. Statistical comparisons were performed between the membranes (ADEs and NDBs), as well as within the membranes (between the GA/PVA ratio in blends, namely 1/0, 1/0.25, 1/0.5, 1/0.75, 1/1, and 0/1). Comparing membranes, there was no statistical difference between the ADBs and NDBs, concerning their particle size (13.57 and 14.77 nm, respectively). On the other hand, comparing the blend ratios within the membrane (Table 3, Figures 7A and 8) revealed that the GA membrane (GA = 100%) had the lowest PS for each of the means (13.57 nm), with a maximum value (55.44 nm). Furthermore, PVA sheets had the highest PS values (20.34 and 89.75 nm for the mean and maximum values, respectively). In between, increasing the PVA concentration in the bioplastic blends increased the PS gradually (Table 3 and Figures 7F and 8).

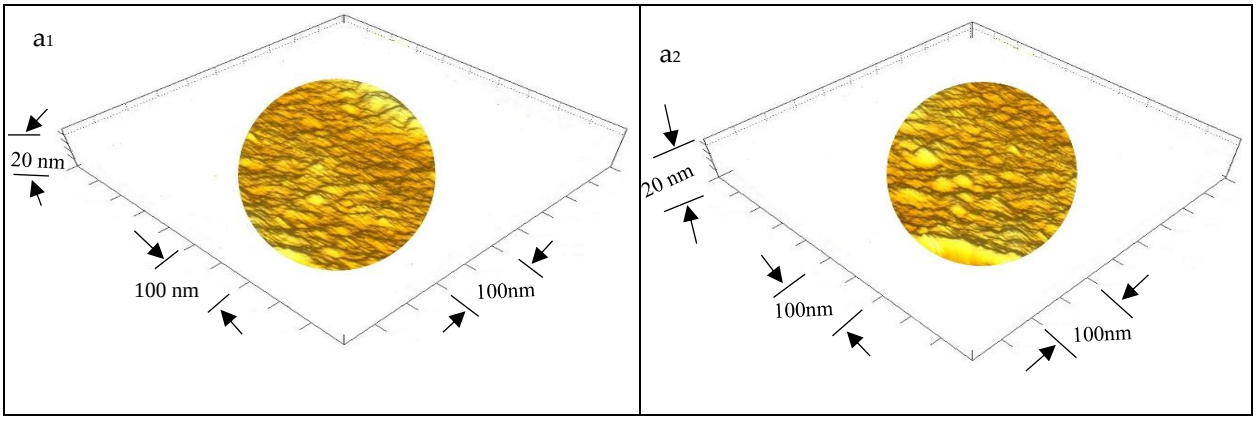

Figure 7. A. AFM images of surface roughness of the bioplastic sheet blended from gum Arabic (GA) precursor: a_1) air-dried membrane (ADB) and a_2) nano-dehydrated bioplastic membrane (NDB).

Preprints (www.preprints.org) | NOT PEER-REVIEWED | Posted: 25 May 2023 doi:10.20944/preprints202305.1803.v1

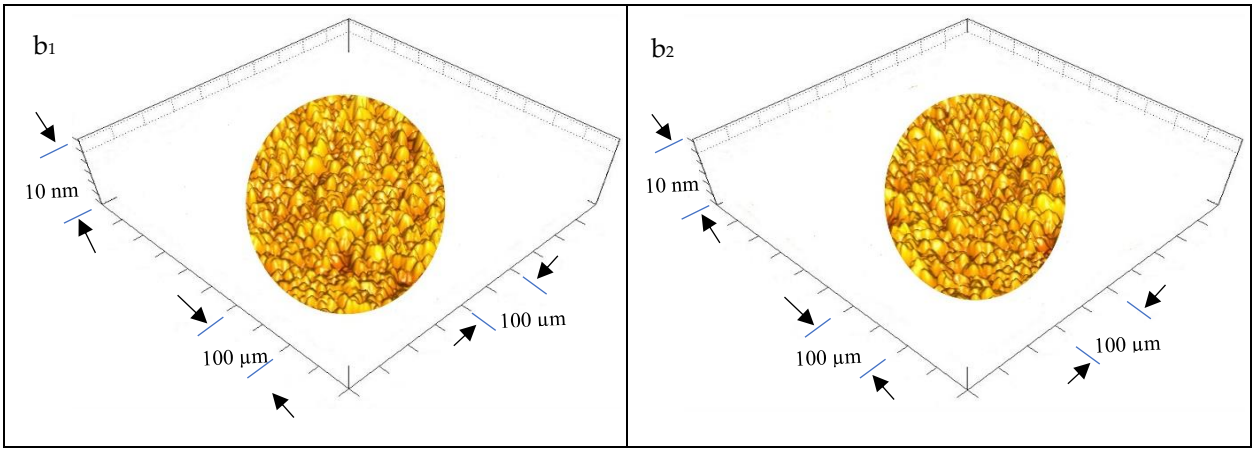

Figure 7. B. AFM images of surface roughness of the two bioplastic sheets blended from GA and polyvinyl alcohol (PVA) precursors (1:0.25): b_1) air-dried membrane (ADB) and b_2) nano-dehydrated bioplastic membrane (NDB).

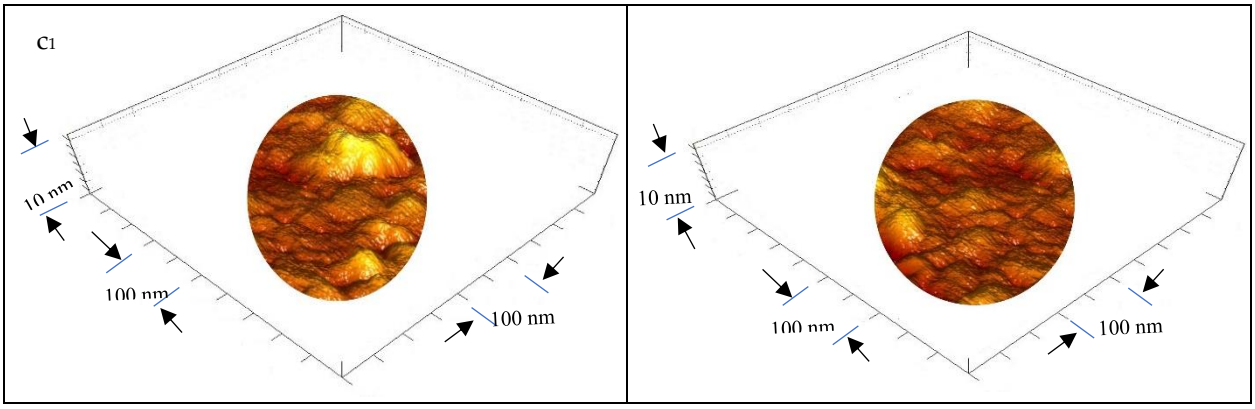

Figure 7. C. AFM images of surface roughness of the two bioplastic sheets blended from GA and PVA precursors (1:0.5): c_1) air-dried membrane (ADB) and c_2) nano-dehydrated bioplastic membrane (NDB).

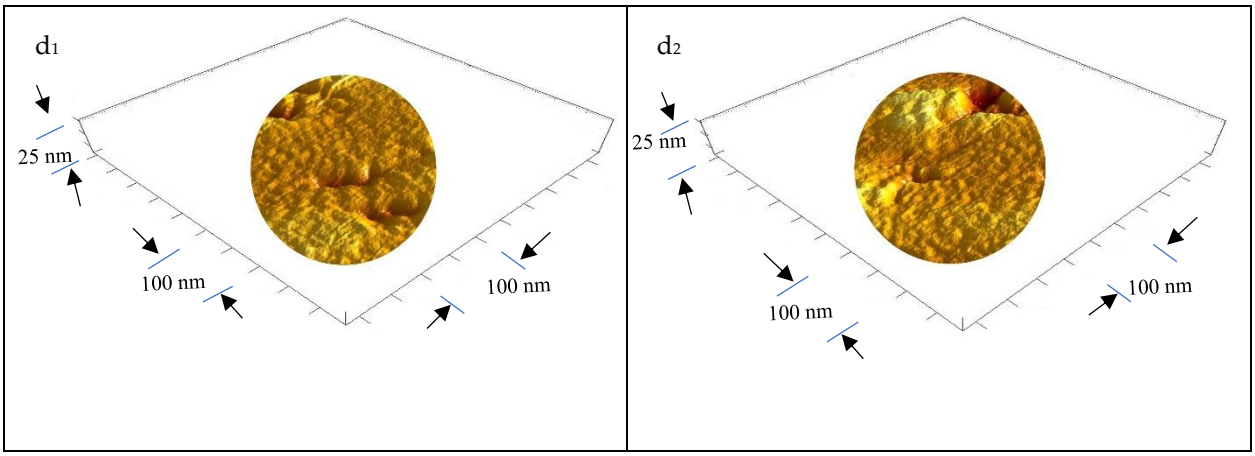

Figure 7. D. AFM images of surface roughness of the two bioplastic sheets blended from GA and PVA precursors (1:0.75): d_1) air-dried membrane (ADB) and d_2) nano-dehydrated bioplastic membrane (NDB).

Preprints (www.preprints.org) | NOT PEER-REVIEWED | Posted: 25 May 2023 doi:10.20944/preprints202305.1803.v1

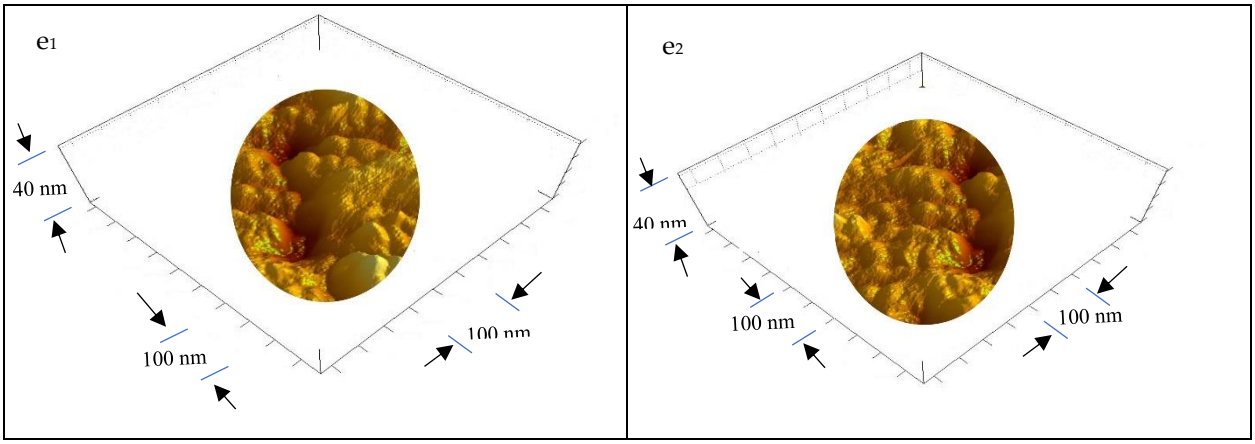

Figure 7. E. AFM images of surface roughness of the bioplastic sheets blended from GA and PVA precursors (1:1): e1) air-dried membrane (ADB) and e2) nano-dehydrated bioplastic membrane (NDB).

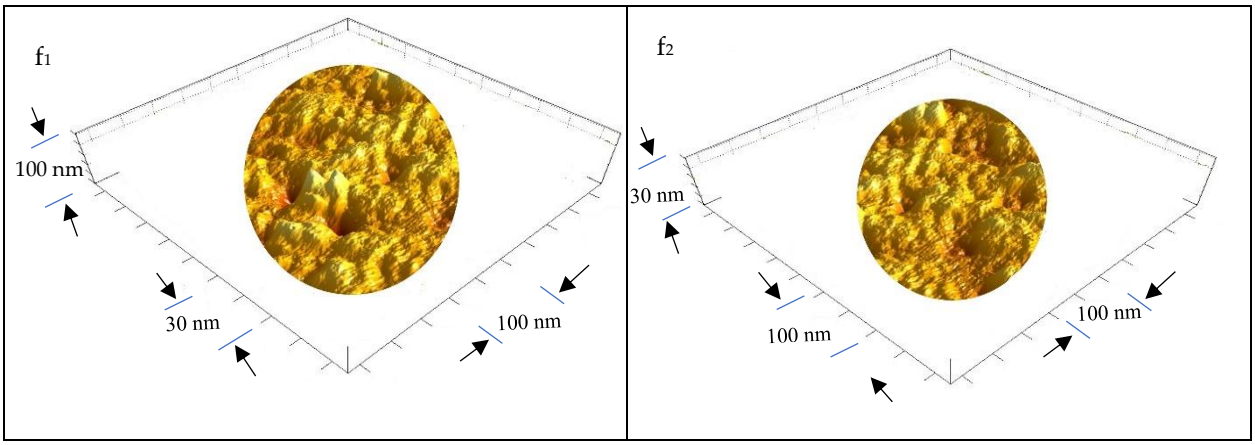

Figure 7. F. AFM image of surface roughness of the bioplastic sheets blended from polyvinyl alcohol (PVA) precursor: f1) air-dried membrane (ADB) and f2) nano-dehydrated bioplastic membrane (NDB).

Table 3. Statistical parameters (SPs) of the ultrastructural features of the bioplastics.

GA/PVA Ratio	GA Amount %	PVA Amount %	SPs	Particle Size nm		Permeability			
						Pore Diameter nm		Void Volume nm³	
				ADB	NDB	ADB	NDB	ADB	NDB
1/0	0	100	Mean [1,2]	13.57	14.77	0.91	0.953	83.24	84.29
			Max. [3]	55.44	56.68	3.905	3.948	1397.9	1398.91
			Min. [4]	4.24	5.49	0.002	0.045	0.007	1.057
			SD [5]	7.66	7.66	0.904	0.904	160.68	160.68
1:0.25	20	80	Mean [1,2]	14.17	15.42	0.553	0.606	105.74	106.74
			Max. [2,3]	76.94	78.19	3.54	3.593	1374.8	1375.47
			Min. [2,4]	4.24	5.49	0.001	0.055	0.005	1.008
			SD	8.93	8.93	0.457	0.457	156.17	156.17
1:0.5	66.7	33.3	Mean [1,2]	15.15	16.4	0.608	0.671	120.66	121.87
			Max. [2,3]	67.01	68.26	2.38	2.443	8009	8010.22
			Min. [2,4]	4.24	5.49	0.001	0.064	0.002	1.219
	100 nm		SD [5]	8.51	8.51	0.469	0.469	309.6	309.6
1:0.75	57.1	42.9	Mean [1,2]	17.01	18.07	0.714	0.788	226.98	228.18
			Max. [2,3]	72.32	73.38	3.608	3.683	8411.8	8412.98

Preprints (www.preprints.org) | NOT PEER-REVIEWED | Posted: 25 May 2023 doi:10.20944/preprints202305.1803.v1

			Min. [2,4]	4.24	5.3	0.007	0.082	0.007	1.215
			SD [5]	9.26	9.26	0.615	0.615	631.41	631.41
1:1	50	50	Mean [1,2]	18.42	19.58	1.145	1.23	460.18	461.5
			Max. [2,3]	89.75	90.91	4.75	4.839	8411.8	8413.1
			Min. [2,4]	4.24	5.4	0.019	0.093	0.007	1.34
			SD [5]	12.69	12.69	2.342	1.002	1062.04	1062.04
0/1	100	0	Mean [1,2]	20.34	21.35	1.485	1.58	548.95	552.41
			Max. [2,3]	89.75	90.76	14.851	14.946	9315	9318.46
			Min. [2,4]	4.24	5.25	0.019	0.114	0.001	3.46
			SD [5]	14.58	14.58	2.342	2.342	1198.36	1198.36

[1] Mean of the population members. [2] The number of observations is 1000 individuals. [3] Max. is the maximum value. [4] Min. is the minimum value. [5] SD are standard deviation values present within the parentheses.

Permeability and Void Volume (PD and VV)

Data produced for both PD and VV are presented in Table 3, in Figures 8B, 9, and S7 for PD, and in Table 3 and Figure 8c for VV. The same ascending trend was noticed for both PD and VV regarding their influence, with an increase in the PVA allocation in the ADBs as well as NDBs. The PD of the ADB increased from 0.91 nm to 1.485 nm for the GA/PVA ratios of 1/0 and 0/1, respectively. In addition, the VV of the ADB increased from 83.24 nm^3 to 548.95 nm^3 for the GA/PVA ratios of 1/0 and 0/1, respectively.

In addition, there was no statistical difference between the ADBs and NDBs in their PS, PD, and VV; consequently, there is no evidence that the novel procedures used in the bioplastic membrane preparation alter their parent ultrastructure.

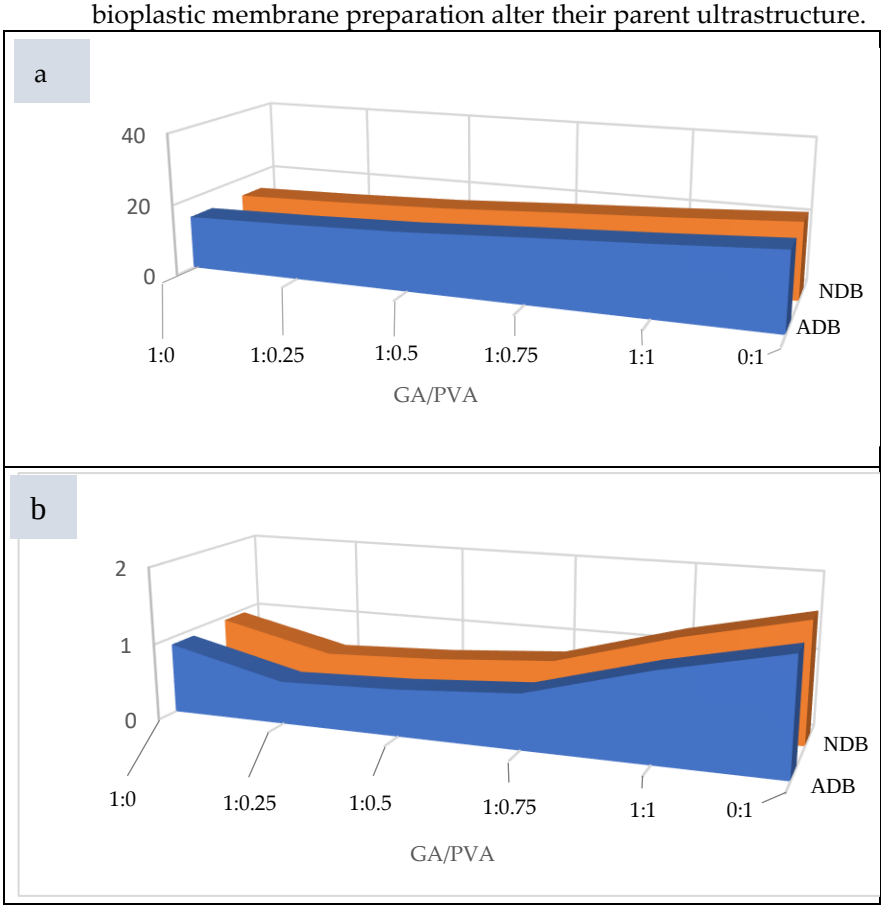

Preprints (www.preprints.org) | NOT PEER-REVIEWED | Posted: 25 May 2023 doi:10.20944/preprints202305.1803.v1

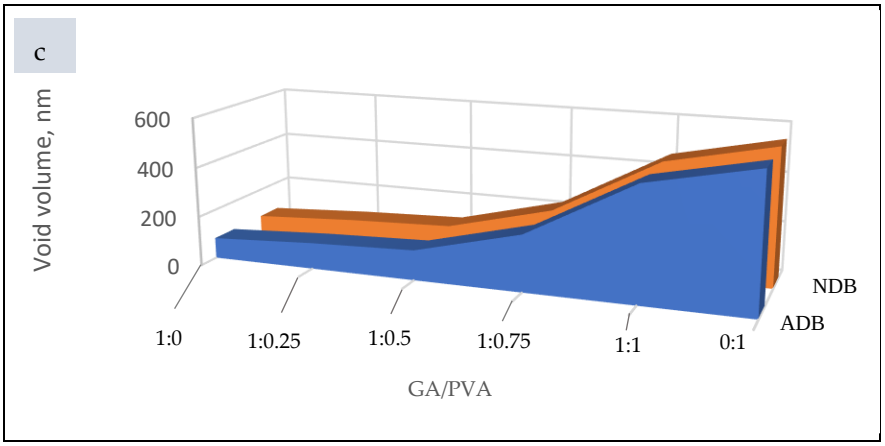

Figure 8. Ultrastructure features of the air-dried membrane (ADB) and the nanodehydrted-bioplastic membrane (NDB): a) particle size, B) pore diameter, and C) void volume as affected by different alloations of GA and PVA (GAPVA blends)

Preprints (www.preprints.org) | NOT PEER-REVIEWED | Posted: 25 May 2023 doi:10.20944/preprints202305.1803.v1

3.1.6. Bacterial and Fungal Biodegradation

The microbial communities for the initial soil samples, as well as the buried bioplastic sheets, were found to be different in number and species (Table 4). Depending on the type of buried membrane, different types of bacteria and fungi were found. *Pseudomonas* spp. [107,108], *Bacillus* spp. [58,107,108], *Aspergillus* spp. [109], and *Penicillium* spp. [107,110] were the predominant species for the buried PVA. *Bacillus* spp. [59,111], *Pseudomonas* spp., *Aspergillus* spp., *Rhizorpous* spp., *Fusarium* spp., *Penicillium* spp., and yeast *Saccharomyces* [59] were additional important species for the buried GA.

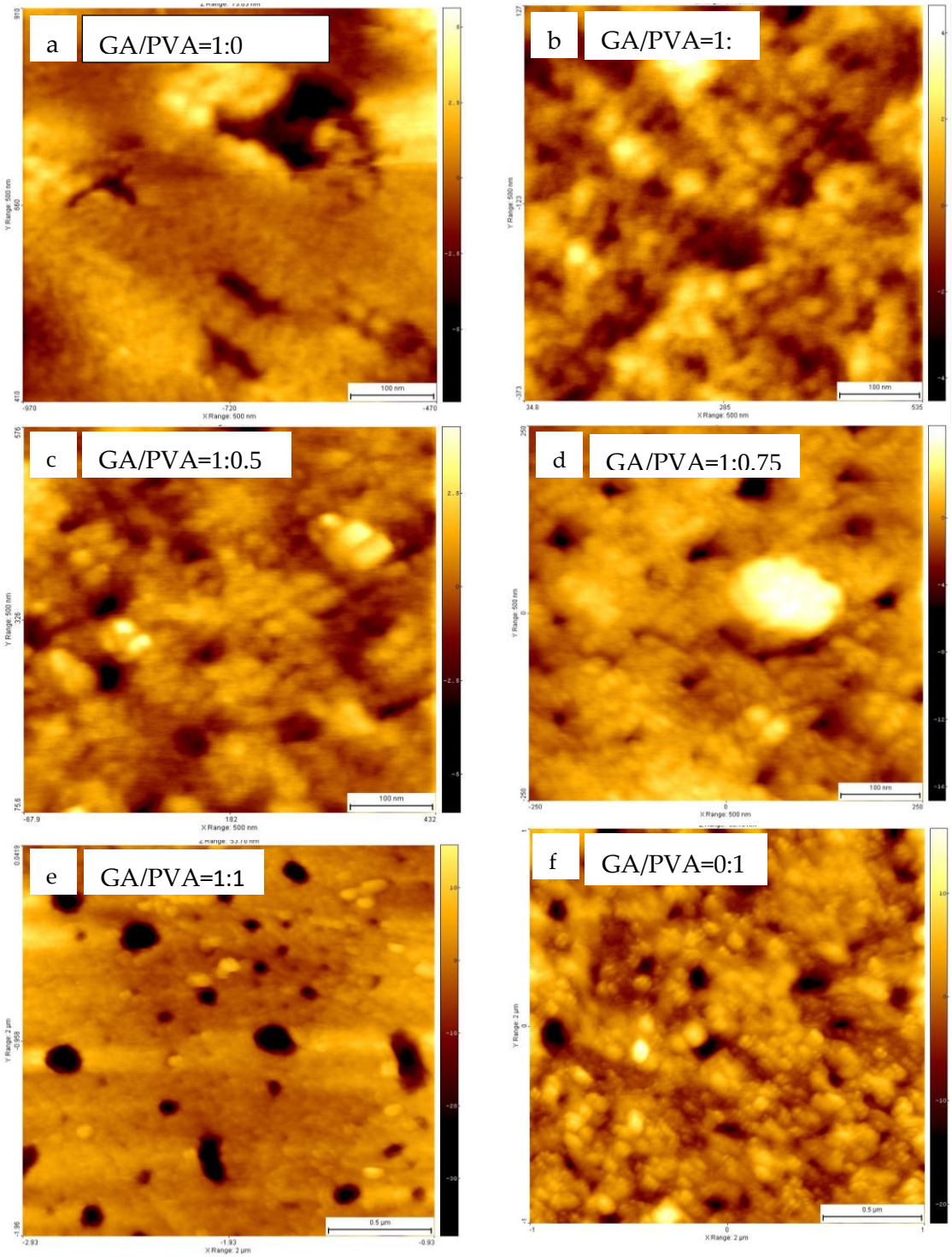

Preprints (www.preprints.org) | NOT PEER-REVIEWED | Posted: 25 May 2023 doi:10.20944/preprints202305.1803.v1

Figure 9. Permeability of the nano-dehydrated bioplastic membranes blended from gum Arabic (GA) and polyvinyl alcohol (PVA) precursors in different ratios of GA/PVA: a) 1/0, b) 1:0.25, c) 1:0.5, d) 1:1.75, e) 1:1, and f) 0/1, respectively (AFM images)

Moreover, the (GA/PVA = 1:1) bioplastic blend's microbial populations included *Bacillus* spp. [58,111], *Pseudomonas* spp., *Aspergillus* spp., *Rhizorpous* spp., *Fusarium* spp., and *Penicillium* spp. In addition, more fungal species than bacteria were found, which is consistent with the findings of Hindi et al. [93], who discovered that fungal isolates had a higher ability to use the sheets as growth substrates than bacteria.

Table 4 contains information about the colony-forming units (CFU) of different microbial species. The total counts of bacteria, fungus, and yeast were determined to be 2.28 × 10^5 and 1.88 × 10^3 CFU/mL, respectively, in the first soil sample, and they were higher than those for GA and PVA (Table 4). After 30 and 60 days, pure GA (100%) had a higher CFU than pure PVA (100%). The CFU values measured after 30 and 60 days for each of the six bioplastic sheets showed no discernible differences.

Table 4. Colony-forming units (CFU) of microbial populations for bacterial and fungal species in the buried NDBs blended from gum arabic (GA) and polyvinyl alcohol (PVA) in different ratios for soil burying.

AG/PVA Ratio	After 30 Days		After 60 Days	
	Bacteria CFU/mL	Fungi CFU/mL	Bacteria CFU/mL	Fungi CFU/mL
GA = 100%	2.8 × 10^6 [0.032] [1]	1.77 × 10^3 [0.008]	6.69 × 10^6 [0.086]	4.32 × 10^3 [0.077]
1:0.25	2.6 × 10^6 [0.07]	1.8 × 10^3 [0.042]	5.86 × 10^6 [0.074]	3.8 × 10^3 [0.093]
1:0.5	2.52 × 10^6 [0.028]	1.88 × 10^3 [0.094]	5.7 × 10^6 [0.064]	4.21 × 10^3 [0.086]
1:0.75	2.5 × 10^6 [0.031]	1.93 × 10^3 [0.095]	5.67 × 10^6 [0.095]	4.02 × 10^3 [0.086]
1:1	2.17 × 10^6 [0.088]	1.9 × 10^3 [0.012]	6.14 × 10^6 [0.088]	3.79 × 10^3 [0.044]
PVA = 100%	1.93 × 10^6 [0.008]	2.1 × 10^3 [0.083]	6.12 × 10^6 [0.093]	4.83 × 10^3 [0.046]
Soil control sample	Bacteria: 2.28 × 10^5 CFU/mL [0.058]			
	Fungi: 1.88 × 10^3 CFU/mL [0.022]			

[1] Values within parentheses are standard deviations.

4. Discussion

4.1. Scientific Illustration of the Ease of Peeling of the Bioplastic Membranes from the Acrylic Substrate

In addition to the issue of drying the bioplastic sheets facing all hydrophilic natural polymers-based membranes, peeling these sheets to be rolled up is a major problem in the hydrophilic bioplastic blend field. Studying the ease of peeling the bioplastic membrane away from the casting panel template was achieved by investigating the chemical and physical properties of each of three parameters, namely the bioplastic blend (fluid phase), the PMMA substrate (solid phase), and the liquid/solid interface, as shown in Figure S4 [57,93,112–117].

Poly-(methyl methacrylate), also known as PMMA, is an acrylic panel material that was used in the current experiment (Figure 1C, and Figures S4 and S5) because it is non-stick with blend materials, and the sheets may be removed from the panels with ease after

 doi:10.20944/preprints202305.1803.v1

drying and curing. In Figure 1D, the resulting clear sheets were stored under dry circumstances until use [57].

Regarding the triboelectric series, which classifies materials based on their propensity to take electrons (tribo-positive) or not (tribo-negative), it is important to note that PMMA is a biocompatible polymer that, due to its propensity for either donating or absorbing electrons, occupies the middle position on the triboelectric series [112].

Due to its non-stick surface, which can prevent the bioplastic blend from being easily peeled, PMMA has been found to be an ideal casting platform for polymers, particularly water-based ones. The following examples show how simple it is to separate the bioplastic membrane from the acrylic substrate:

a. Materials with relatively low surface energies are regarded as non-stick surfaces [118] and vice versa. As shown in Table S5, the acrylic substrate exhibits modest surface energy (41 dynes/cm) and contact angle (82°), both of which are indicative of a non-stick surface.
b. Acrylic is a powerful static generator in terms of electrostatic charge. When its surface is wiped back and forth, positive and negative surficial charges arise that draw and hold microscopic particles. Surficial charge variations have the potential to cause agglomerated particles to discharge in an unanticipated manner, endangering contamination-sensitive materials [120]. PMMA is positioned close to the middle of this empirical series for the surface potential and is regarded as a tribo-positive electron-donating material [112,120].

GA is composed of three distinct fractions, as shown in Figure S4, including arabinogalactan-protein complex (MW 1500 kDa; approximately 10% of the total gum solids), arabinogalactan (MW 280 kDa; approximately 88% of the total gum solids), and glycoprotein (MW 250 kDa; approximately 2% of the total gum solids [121–123]. Due to its low molecular weight and branching pattern, arabinogalactan films are challenging to produce [124,125].

According to Winiewska et al. [126], PVA chains have a particular percentage of acetate groups (14%), which are the source of the polymer molecules negative charges. The structure of the PVA adsorption layer is impacted by even the comparatively modest portion of these groups. The presence of more acetate groups in the polymeric chains resulted in increased PVA adsorption levels, indicating that these groups are crucial to PVA adsorption [127]. As the pH of the solution rises, so does the contribution of charged acetate groups.

Due to the electrostatic attraction of negative charges present along the polymeric chains, the polymer chains extend further. The amount of PVA is directly influenced by the degree of development in the polymer macromolecules.

In general, plastics are categorized into four categories by Nuraje et al. [128]: superhydrophilic, hydrophilic, hydrophobic, and superhydrophobic, with contact angles (Θ) of below 5°, below 90°, 90°–150°, and 150°–180°, respectively.

The liquid–fluid–solid system exhibits three different interfaces in its configuration when a liquid drop is placed on a solid surface (Figure S4), namely liquid–fluid, solid–fluid, and liquid–solid. It is noticed that adhesive and cohesive forces are present at each interface as a result of the intermolecular forces at work there. Cohesive forces cause the drop to return to its spherical shape, whereas adhesion forces encourage it to spread out. The conflict between these two forces determines the contact angle [57,73,126,130]. It is feasible to establish a connection between the static contact angle and the interfacial stresses under equilibrium conditions. The Young–Dupre equation is the name of this relationship.

By applying the Hild [131] formula, it was discovered that the spreading of a droplet of a bioplastic blend is equal to A − (B + C), where A is the surface tension of the bioplastic blend, B is its surface tension, and C is the surface energy of the interface between the bioplastic blend and the acrylic panel. While liquid will spread when the spreading is zero to positive, it will not if the spreading is negative.

Preprints (www.preprints.org) | NOT PEER-REVIEWED | Posted: 25 May 2023 doi:10.20944/preprints202305.1803.v1

4.2. Chemical and Physical Properties of the Bioplastic Membranes

4.2.1. FTIR

Different organic functional groups found in naturally occurring substances can be recognized using Fourier transform infrared (FTIR) spectroscopy. The complicated vibrational modes were seen in the FTIR spectra for the various bioplastic samples over a wide range of wavenumbers (Figure 3).

Figure 3 shows the strong and broad O-H stretching vibrations at 3416 cm^{-1} dominating the primary FTIR spectra of the six bioplastic sheets. At 2939 cm^{-1}, the C-H stretching modes are riding above the board peak. Along with the bulk ring mode at 1426 cm^{-1}, the carbonyl stretching modes are seen at 1641 cm^{-1}. At 1047 cm^{-1}, the typical C-O-C anti-symmetric stretching mode was found. These findings are modified with those attained by other researchers [103–106] for the study of biopolymeric materials.

For additional illustration, the overall banding of the FTIR analysis showed a carbohydrate fingerprint at 900–1250 cm^{-1} [132]; C–O–C anti-symmetric stretching at 1426 and 1047 cm^{-1} [57,93,94]; COO^- asymmetric stretching at 1402 cm^{-1} [133]; an O–H in-plane bending band in carboxylic acids at 1625.4, 1627.4, 1430, 1436.91, and 1437 cm^{-1} [133,134]; COO^- symmetric stretching and carbonyl stretching modes at 1641 cm^{-1} [57,93,94,96]; C–H stretching at 2800–3000, 2885, and 2939 cm^{-1} [57,93,94,96,130,133,134]; vibrational modes of the C–H group at 2910.87 cm^{-1} [134,135]; O–H stretching vibrations at 3261, 3416, and 3000–3600 cm^{-1} [57,93,129,133,135], and the unique presence of O–H groups at 3526.35 cm^{-1} [133,134].

The FTIR for the TBM used in the current work, and the ADB created by Hindi et al. [93] have main functional groups that share chemical characteristics, according to the comparison. As a result, the chemical components of the bioplastic products have been preserved by the use of innovative casting blends, nanodehydration, and membrane peeling.

4.2.2. XRD

The GA-broad diffractogram's greatest intensity was recorded at 2 = 20° (Figure 4), which supports the amorphous nature of gum arabic [13]. Moreover, a typical peak for pure PVA, a semi-crystalline polymer detected at 2 = 19.9° (Figure 4f), confirmed its semi-crystallinity feature [57,93,106].

With the increase in PVA allocation in the blend, the crystallinity index values increased. The growing CI of the bioplastic blends can be correlated to the increasing PVA allocation in the blend because the CI value of PVA (54.81%) was found to be greater than that of GA (19.4%).

4.2.3. TGA

TGA analyzes the mass change behavior in bioplastic membranes that occur as a function of temperature and time in a controlled environment. The best uses for it are to evaluate reaction kinetics, volatile contents, thermal stability, degradation traits, aging/lifetime breakdown, and degradation features.

The thermal deterioration of the samples increased at higher temperatures (up to 500 °C) than at the lower temperatures, according to a comparison of the mass losses between the temperature zones. Furthermore, a comparison of the mass losses across the temperature ranges revealed that PVA shed more weight at the higher temperature zones than GA. A mass loss of up to 100 °C can be attributed to the water molecule's large solvation capacity, which results in the evaporation of loosely bound moisture on the surface, or "free water" [136]. Furthermore, mass loss at temperatures up to 150 °C can be due to hygroscopic water evaporation [57,93].

4.2.4. DTA

Similar information is provided by the DTA, which measures the temperature difference between a sample and a reference due to thermal treatments in a material. The DTA typically provides phase transition information in addition to TGA.

 doi:10.20944/preprints202305.1803.v1

It is commonly known that two types of thermograms can be distinguished for a given material during thermal reactions: endothermic, which uses energy, and exothermic, which excludes energy. The depolymerization of the bioplastic materials themselves as a result of heat treatment causes exograms to occur (Figure 6). Moreover, the endotherm can be attributed to the fusing or melting of crystallites, as well as the evaporation of free moisture (up to 100 °C) and hygroscopic moisture (up to 120 °C) [57].

As shown in Figure 6 and Table 2, GA had the lowest value of heat change (−1017.3 Vs/mg), but the endotherm of pure PVA absorbed the maximum amount of energy (2119.7 Vs/mg) among the other bioplastic blends. As a result, PVA is more thermally stable than GA because it absorbs heat more effectively, shielding the bioplastic sample from potential thermal degradation brought on by rising temperatures. Moreover, the enhanced PVA allocation in the blends boosted the thermal stability of the bioplastic sheets.

GA exhibits greater thermal stability than PVA at higher temperatures (about 350 °C). As a result, altering a bioplastic blend to increase PVA or decrease GA enhances the thermal stability of the resulting bioplastic membrane [57,93].

4.2.5. Surface Roughness and Nanometric Particle Size

While the pure PVA sheets (0/1 blend ratio) had the greatest PS values for both the ADB and TBM, the pure GA membrane (1/0) had the lowest PS values, gradually raising the PVA concentration in the bioplastic blend increased the PS. The surface roughness (SR) features examined via atomic force microscopy (AFM), as shown in Table 3 and Figure 7A–F, provide a confirmation of this. The results obtained for PVA-based membranes with the median value for those cast from the GA/PVA (1:1) are compared.

As a result, the presence of PVA causes the SR of the water-based polymeric blends to increase, generating a surface that is rougher. This is supported by the surface roughness features examined using atomic force microscopy (AFM), as shown in Table 3 and Figure 7.

Increases in PVA allocation make the blend's texture coarser since PVA membranes have a rougher structure than GA membranes. There is no statistically significant difference between the ADB and TBM in their PS, along with the six bioplastic blends, according to the comparison of the membranes. Additionally, analyses of the effects of different bioplastic blend ratios on a membrane showed that, in both cases, blends with higher PVA concentrations produced membranes with higher porosities (PD and VV).

It is important to note that smoother sheets are preferred for packaging than coarser ones because the latter tend to gather more dust on their surfaces. Although PVA is a crucial part of the bioplastic mixture that improves the quality of the final membrane and makes it easier for it to peel off the casting surface after drying, a careful balance must be taken into account to have the best quality and smoothest surfaces.

Moreover, there is no statistical distinction in the PS between the ADB and TBM. Because of this, the unique techniques created to make it easier to cast their mixes, dry them faster, and peel membranes off easily using a self-electrostatic template did not alter the parent roughness properties. Because of this, the unique approaches employed in the current study did not alter the permeabilities of the membranes (PD and VV).

4.2.6. Membrane Permeability

For membrane ultrastructure, the GA membranes had the lowest PD and VV compared to those for PVA, which had the highest ones for both air-dried bioplastic membrane (ADB) and nanodehydrated transparent bioplastic membrane (TBM). Accordingly, increasing the PVA allocation increased the membrane permeability, which facilitated the water evaporation from the blend upon the nanodehydration procedures.

When compared to PVA membranes, which had the highest PD and VV for both the air-dried bioplastic (ADB) and nanodehydrated TBM membranes, the GA membranes had the lowest ultrastructures. As a result, increasing the PVA allocation also increased

 doi:10.20944/preprints202305.1803.v1

the membrane permeability, which made it easier for the blend's water to evaporate throughout the nanodehydration processes.

Moreover, there is no statistical difference between the ADB and TBM for eah ase of the PS, PD, and the VV. Because of this, the unique approaches employed in the current study did not alter the permeability of the membranes (PD and VV), as shown in Figure 8 and Table 3.

4.2.7. Microbial Biodegradation

Biodegradation of the TBM material was confirmed significantly by its reduction in weight for all of the six TBM samples, and it was found that degradation commenced within 30 and 60 days.

The microbial communities in all the buried bioplastic sheets, including the control one, were different in number and species. The species of bacteria and fungi differed according to the type of buried sheet.

The microbiological study revealed that all six bioplastic sheets are able to be degraded, contrary to petroleum-based sheets.

Biodegradation is the process where microorganisms can degrade bioplastic membrane materials, leading to a loss of weight after a period of time. Our results show that all blended bioplastic membranes had reduced weight, especially GA. Our results agree with Sasaki et al. [87], who prepared films of phenolic extracts incorporated into GA and found that the highest weight loss of films was 45.81%, compared with GA (26.87%) after 30 days.

Microorganisms can degrade bioplastic membranes through a process called biodegradation, which eventually causes the membranes to lose weight. Our findings indicate that the weights of all blended bioplastic membranes, particularly GA, decreased. Our findings are consistent with those of Sasaki et al. [87], who created films using phenolic extracts mixed with GA and discovered that after 30 days, the weight loss of the films was higher than that of the GA (45.81%).

These findings were contrary to Ibrahim [80], who discovered that for nanofiber membranes based on homogenous polymeric blends of gum arabic, polyvinyl alcohol, and silver nanoparticles, the biodegradation tests of the generated nanofibers revealed that 99.09% of the material was broken down after 28 days. These variations in the results can be explained by the fact that a variety of factors, including microbes, humidity, sunshine, and oxygen, can affect the bioplastic's capacity to degrade [74].

In addition, because it affects the microbial population and shapes it, the depth of the soil that bioplastic membranes are buried in is a crucial component for biodegradation [81]. In addition, as a result of using gum as a source of nutrients, the number of bacteria increased over time [76,93].

Our results proved that *Pseudomonas* spp., *Bacillus* spp., and *Micrococcus* spp. were the most commonly isolated bacterial strains appearing in different samples, while *Rhizobus* spp., *Penicillium* spp., and *Fusarium* spp. were the most commonly isolated fungus strains that appeared in our different samples. These findings agree with those found by Santos-Beneit et al. [88] and Sasaki et al. [87], which were isolates of *Bacillus cereus, Bacillus polymyxa, Bacillus licheniformis, Corynebacterium xerosis, Staphylococcus epidermis, Streptococcus bovis*, and the fungi *Penicillium notatum, Rhizopus nigricans, Aspergillus niger,* and *Fusarium moniliforme* from gum arabic [62,82,84,85,87,136,137].

A common trend was registered between the TBM produts fabricated in the current investigation and the ADB synthesized by Hindi et al. [93] and Hindi and Albureikan [57]. Accordingly, the nanodehydration invention did not affect the parent's ability to biodegrade the bioplastic membranous product.

PVA had a higher crystallinity index (CI), a greater mass loss at higher temperatures, higher thermal stability due to its higher heat content, and greater clearance of surface roughness due to its high particle size (PS), as well as higher permeability parameters,

 doi:10.20944/preprints202305.1803.v1

namely pore diameter (PD) and void volume (VV), than those for GA. Accordingly, increasing the PVA allocation in the bioplastic blends could enhance their properties except for mass loss, whereby increasing the GA allocation in the TBM blend reduced its mass loss at elevated temperatures. The nanodehydration method gave the best solution for the fast drying of any water-based biopolymers, as well as producing free air bubble-sheets with the simple machinery required and easy casting and peeling tasks, besides its wonderful biodegradation behavior when buried in wetted soil.

5. Conclusions and Future Perspectives

- Great success was achieved for the fabrication of bioplastic membranes from gum arabic mixed with polyvinyl alcohol by applying a novel casting method, termed static vibrated-free horizontal flow (VFHF), producing free air bubble sheets.
- The novel nanodehydration technique gave the best solution for drying the bioplastic sheets.
- This is the first time that an acrylic (poly(methyl methacrylate)) panel used as an ideal template surface has had an electrostatically charged hydrophobic surface. As a result, peeling off its template surface is made simpler.
- The novel technique invented and applied in the current investigation can be used for any water-based biopolymeric-based products.
- The most important properties of the nanodehydrated bioplastic membranes were studied using Fourier transform infrared spectroscopy, X-ray powder diffraction, thermogravimetric analysis, differential thermal analysis, and atomic force microscopy, to ensure that the novel techniques did not distort the product quality.
- The TBM retained its parent properties, including chemical functional groups, crystallinity index, mass loss, thermal stability, ultrastructure features (surface roughness and permeability), and its ability for microbial biodegradation.
- The addition of polyvinyl alcohol to the gum arabic enhanced the formation of sheets and their properties, including the crystallinity index and thermal stability, except for mass loss upon elevated temperatures.
- There is no statistical difference between the TBM membranes and ordinary air-dried bioplastic membranes in terms of their particle size and permeability, indicating that the novel procedures used did not distort the parent properties examined, as well as their ability for biodegradation.
- The biodegradation of the TBM material was confirmed significantly by the reduction in weight for all of the six TBM samples, and degradation was found to start within 30 and 60 days.
- *Pseudomonas* sp., *Bacillus* sp., and *Micrococcus* sp. were the most commonly isolated bacterial strains that appeared in different samples, while *Rhizobus* sp., *Penicillium* sp., and *Fusarium* sp. were the most commonly isolated fungus strains that appeared in different samples. Pure GA was the most commonly biodegraded sample among the other bioplastic samples.
- The microbial communities in all of the buried bioplastic sheets, including the control sample, were different in number and species, and the species of bacteria and fungi differed according to the type of buried sheet.
- The microbiological survey revealed that all of the six bioplastic sheets are able to be degraded, contrary to petroleum-based sheets.

6. Patent

System, apparatus, and methods for manufacturing biodegradable biopolymeric materials (US Patent no. 11548192).

Supplementary Materials: The following supporting information can be downloaded at: www.mdpi.com/xxx/s1, Figure S1: title; Table S1: title; Video S1: title.

 doi:10.20944/preprints202305.1803.v1

Author Contributions: Supervision, conceptualization, validation, methodology, and characterization, S.S.H.; planning, revising, and validating all bacterial topics, M.O.I.A. All authors have read and agreed to the published version of the manuscript.

Funding: This work was funded by the Deanship of Scientific Research (DSR), KAU, Jeddah, under grant no. G: 85/155/1434.

Institutional Review Board Statement: Not applicable.

Informed Consent Statement:

Data Availability Statement: The supporting data for the reported results, including a link to the publicly archived datasets analyzed or generated during the study, can be found under the following patent: US Patent for System, apparatus, and methods for manufacturing biodegradable biopolymeric materials (Patent #11548192, issued 10 January 2023)—Justia Patents Search, https://patents.justia.com/patent/11060208 (accessed on 17 November 2022).

Acknowledgments: The authors are deeply thankful to DSR, KAU, Jeddah for funding this research work. The project that revealed this invention was funded by the Deanship of Scientific Research (DSR), King Abdulaziz University, Jeddah, under grants no. 85/155/1434 and, respectively. The authors therefore acknowledge with thanks the DSR for technical and financial support. Appreciation is given to the Center of Nanotechnology (CN) for its technical assistance.

Conflicts of Interest: The authors declare no conflicts of interest.

Nomenclature

Abbreviation	Definition
ADB	Air-dried bioplastic membrane
ACS	The American Chemical Society
AFM	Atomic force microscopy
CI	Crystallinity index
DSC	Differential scanning calorimetry
DTA	Differential thermal analysis
FTIR	Fourier transform infrared spectroscopy
VFHF	Vibrated-free horizontal flow
GA	Gum arabic
HC	Heat change in μVs/mg
TBM	Transparent bioplastic membrane
NPS	Nanometric particle size
PubChem	An open chemistry database managed by the National Institutes of Health (NHI)
PVA	Polyvinyl alcohol
SD	Standard deviation
SEP	Self-electrostatic peeling
SP	Statistical parameters
SR	Surface roughness
PD	Pore diameter
PS	Particle size
TGA	Thermogravimetric analysis
TR	Temperature range (°C)
XRD	X-ray diffraction
VV	Void volume

References

1. Mergaert, J.; Anderson, C.; Wouters, A.; Swings, J.; Kersters, K. Biodegradation of polyhydroxyalkanoates. *FEMS Microbiol. Lett*. **1992**, 9, 317-321.
2. Nampoothiri, K.M.; Nair, N.R.; John, R.P. An overview of the recent developments in polylactide (PLA) research. *Bioresour. Technol*. **2010**, 101, 8493-8501.
3. Boyandin, A.N.; Prudnikova, S.V.; Filipenko, M.L.; Khrapov, E.A.; Vasil'ev, A.D.; Volova, T.G. Biodegradation of polyhydroxyalkanoates by soil microbial communities of different structures and detection of PHA degrading microorganisms. ***Appl. Biochem. Microbiol*. 2012**, 48, 28-36.
4. Merugu, R. Studies on PHB (Polyhydroxy butyrate) degradation by some species of Aspergillus. *Studies*. **2012**, 4, 1111-1113.
5. Gautam, N.; Kaur, I. Soil burial biodegradation studies of starch grafted polyethylene and identification of Rhizobium meliloti therefrom. *J. Environ. Chem. Ecotoxicol*. **2013**, 5, 147-158.
6. Karamanlioglu, M. Environmental degradation of the compostable plastic packaging material poly (lactic) acid and its impact on fungal communities in compost. PhD thesis, Manchester University, UK. **2013**, 198.
7. Badreldin H.A.; Al-Husseni, I.; Beegam, S.; Al-Shukaili, A.; Nemmar, A.; Schierling, S.; Queisser, N.; Schupp, N. Effect of gum Arabic on oxidative stress and inflammation in adenine–induced chronic renal failure in rats. *PLoS One*. **2013**, 8, e55242.
8. Feddersen, R.L.; Thorp, S.N. Sodium carboxymethyl cellulose. In Whistler, R.L.; Bemiller, J.N. (Eds.), Industrial gums, polysaccharides and their derivatives. *Academic Press*. New York. **1993**, 537–578.
9. Verbeken, D.; Dierckx, S.; Dewettinck, K. Exudate gums: occurrence, production, and applications. *Appl. Microbiol. Biotechnol*. **2003**, 63, 10-21.
10. Williams, P.A.; Phillips, G.O. Handbook of Hydrocolloids. Williams, P. A., Phillips, G. O., Eds.; *CRC Press*, Cambridge, *Elsevier*. **2000**, 155-168.
11. Anonymous[a]. FAO Rome. Food and Nutrition. Food and Agriculture Organization, Rome. **1990**, 49.
12. Buffo, R.A.; Reineccius, G.A.; Oehlert, G.W. Factors affecting the emulsifying and rheological properties of gum acacia in beverage emulsions. *Food Hydrocoll*. 2001, 15, 53-66.
13. Almuslet, N.A.; Hassan, E.A.; Al-Sherbini, A.A.M.; Muhgoub, M.G.A. Diode laser (532 nm) induced grafting of polyacrylamide onto gum Arabic. *J. Phys. Sci*. **2012**, 23: 43–53.
14. Anonymous[b]. Network, Kenya. Production and marketing of gum Arabic. Nairobi, Kenya: for natural gums and resins in Africa (NGARA). **2016**.
15. Krempel, M.; Griffin, K.; Khouryieh, H. Hydrocolloids as emulsifiers and stabilizers in beverage preservation. The science of beverages. Grumezescu, A.M.; Holban, A.M. (Eds). Preservatives and preservation approaches in beverages, *Academic Press*. 2019, 15, 427-465.
16. Rinsky, L.H.; Rinsky, G. The Pastry chef's companion: A comprehensive resource guide for the baking and pastry professional. Chichester: John Wiley & Sons. **2009**, 1, 134.
17. Maqbool, M.; Ali, A.; Alderson, P.G.; Zahid, N. Exploring the new applications of gum Arabic obtained from acacia species to preserve fresh fruits and vegetables. II International Symposium on underutilized plant species: Crops for the future - beyond food security, Kuala Lumpur, Malaysia. **2013**, 2, 2406-6168.
18. McEachran, Rich. Gum Arabic: the invisible ingredient in soft drink supply chains. *The Guardian*. **2013**. Available online: www.theguardian.com (accessed on 16 February 2023).
19. Anderson, D.M.W.; Farquhar, J. G. K. Gum exudates from the genus Prosopis. *Int. Tree Crops J*. **1982**, 2, 15-24.
20. Anderson, D.M.W.; McNab, C.G.A.; Anderson, C.G.; Brown, P.M.; Pringuer, M.A. Studies of uronic acid materials, Part 58: Gum exudates from the genus Sterculia (gum karaya). *Int. Tree Crops J*. **1983**, 2, 147-154.
21. Suliman, S.M.; Hamdouk, M.I.; Elfaki, M.B. 2000. Gum Arabic fibre as a supplement to low protein diet in chronic renal failure patients. Sudan Association of Physicians, 17th Conference, Friendship Hall, Khartoum, Sudan, March 21–23.
22. Gamal el-din, A.M.; Mostafa, A.M.; Al-Shabanah, O.A.; Al-Bekairi, A.M.; Nagi, M.N. Protective effect of Arabic gum against acetaminophen-induced hepatotoxicity in mice. *Pharmacol. Res*. **2003**, 48, 631–635.
23. Eltayeb, I.B.; Awad, A.I.; Elderbi, M.A.; Shadad, S.A. Effect of gum Arabic on the absorption of a single oral dose of amoxicillin in healthy Sudanese volunteers. *The Journal of J. Antimicrob. Chemother*. **2004**, 54, 577–8.
24. Ali, A.A.; Ali, K.E.; Fadlalla, A.; Khalid, K.E. The effects of gum Arabic oral treatment on the metabolic profile of chronic renal failure patients under regular haemodialysis in central Sudan. *Nat. Prod. Res.* **2008**, 22, 12–21.
25. Hills, S. Gum Arabic caloric value lowered. 2008. Available online: www.foodnavigator-usa.com (accessed on 24 January 2023).
26. Ali, B.H.; Ziada, A.; Blunden, G. Biological effects of gum Arabic: a review of some recent research. *Food Chem. Toxicol*. **2009**, 47, 1-8.
27. Omer, A.E.; Ayed, I.A.M.; El Badwi, S.M.A. 2013. Effect of gum Arabic on nephrotoxicity induced by *Aristolochia bracteolata* in rats. *Scholars Acad. J. Biosci*. **2013**, 1, 377–380.
28. Luo, Y.; Zhang, Y.; Pan, K.; Critzer, F.; Davidson, P.M.; Zhong, Q. Self-emulsification of alkaline-dissolved clove bud oil by whey protein, gum Arabic, lecithin, and their combinations. *J. Agric. Food. Chem*. **2014**, 62, 4417–4424.
29. Wang, H.; Williams, P.A.; Senan, C. Synthesis, characterization and emulsification properties of dodecenyl succinic anhydride derivatives of gum Arabic. *Food Hydrocoll*. **2014**, 37: 143-148.
30. Lawrence, R.; Jeyakumar, E.; Gupta, A. Antibacterial activity of Acacia Arabica (Bark) extract against selected multi drug resistant pathogenic bacteria. *Int. J. Curr. Microbiol. Appl. Sci*. **2015**, 1, 213–222.

 doi:10.20944/preprints202305.1803.v1

31. Hadavi, M. et al. Novel calcified gum Arabic porous nano-composite scaffold for bone tissue regeneration. *Biochem. Biophys. Res. Commun*. **2017**, 488, 671-678.
32. Salih, N.K. Applications of gum Arabic in medical and health benefits. In gum Arabic. *Academic Press*. **2018**, 269-281.
33. Kraaijpoel, D.; Herenius, C. Het kunstschilderboek-handboek voor materialen en technieken, Cantecleer. **2007**, 183.
34. Banerjee, S.S.; Chen, D.-H. Magnetic nanoparticles grafted with cyclodextrin for hydrophobic drug delivery. *Chem. Mater*. **2007**, 19, 6345–6349.
35. Wilson Jr., O.C.; Blair, E.; Kennedy, S.; Rivera, G.; Mehl, P. Surface modification of magnetic nanoparticles with oleylamine and gum Arabic. *Mater. Sci. Eng. C*. **2008**, 28, 438–442.
36. Kattumuri, V.; Katti, K.; Bhaskaran, S.; Boote, E.J.; Casteel, S.W.; Fent, G.M.; Robert-son, D.J.; Chandrasekhar, M.; Kannan, R.; Katti, K.V. Gum Arabic as a photochemical construct for the stabilization of gold nanoparticles: in vivo pharmacokinetics and X-ray-contrast-imaging studies. *Small*. **2007**, 3: 333–341.
37. Kumar, M.K.; Reddy, A.L.M.; Ramaprabhu, S. Exfoliated single-walled carbonnnanotube-based hydrogen sensor. *Sens. Actuators B*. **2008**, 130, 653–660.
38. Park, C.; Lim, K.H.; Kwon, D.; Yoon, T.H. Biocompatible quantum dot nanocolloids stabilized by gum Arabic. *Bull. Kor. Chem. Soc*. **2008**, 29, 1277–1279.
39. Razzak, M.T.; Darwis, D. Irradiation of polyvinyl alcohol and polyvinyl pyrrolidone blended hydrogel for wound dressing. *Radiat. Phys. Chem*. **2001**, 62, 107-113.
40. DeMerlis, C.C.; Schoneker, D.R. Review of the oral toxicity of polyvinyl alcohol (PVA). *Food Chem. Toxicol*. **2003**, 41, 319-326.
41. Dos Reis E.F.; Campos F.S.; Lage A.P.; Leite R.C.; Heneine L.G.; Vasconcelosc W.L.; Portela Lobato Z.I.; Mansur H.S. Synthesis and characterization of Poly (Vinyl Alcohol) Hydrogels and Hybrids for rMPB70 Protein Adsorption. *Mat. Res*. **2006**, 9, 185-191.
42. Nair, N.R.; Nampoothiri, K.M.; Pandey, A. Preparation of poly (L-lactide) blends and biodegradation by Lentzea waywayandensis. *Biotechnol. Lett*. **2012**, 34, 2031-2035.
43. Liu, M.; Guo, B.; Du, M.; Jia, D. Drying induced aggregation of halloysite nanotubes in polyvinyl alcohol/halloysite nanotubes solution and its effect on properties of composite film. *Appl. Phys. A*. **2007**, 88, 391-395.
44. Masti S.P.; Chougale, R.B. Influence of Poly (Vinylpyrrolidone) on Binary Blend Films Made from Poly(Vinyl Alcohol)/Chitosan. *Inter. Res. J. Env. Sci*. **2014**, 3 11-13.
45. Limpan, N.; Prodpran, T.; Benjakul, S.; Prasarpran, S. Influences of degree of hydrolysis and molecular weight of poly (vinyl alcohol), PVA on properties of fish myofibrillar protein/PVA blend films. *Food Hydrocoll*. **2012**, 29, 226-233.
46. Qiu, K.; Netravali, A.N. Fabrication and characterization of biodegradable composites based on microfibrillated cellulose and polyvinyl alcohol. *Compos. Sci. Technol*. **2012**, 72, 1588-1594
47. Qiu, K.; Netravali, A.N.A Composting study of membrane-like polyvinyl alcohol based resins and nanocomposites. *J Polym Environ*. **2013[a]**, 21, 658-674.
48. Qiu, K.; Netravali, A.N. Halloysite nanotube reinforced biodegradable nanocomposites using noncrosslinked and malonic acid crosslinked polyvinyl alcohol. *Polym. Compos*. **2013[b]**. 34, 799-809.
49. Mudigoudra, B.S.; Masti, S.P.; Chougale, R.B. Thermal behavior of poly (vinyl alcohol). Poly (vinyl pyrrolidone)/chitosan ternary polymer blend films. *Res. J. Recent Sci.* **2012**, 1, 83-86.
50. Onyari, J. M.; Mulaa, F.; Muia, J.; Shiundu, P. Biodegradability of poly (lactic acid), preparation and characterization of PLA/gum Arabic blends. *J Polym Environ*. **2008**, 16, 205-212.
51. Cozic, C.; Picton, L.; Garda, M.R.; Marlhoux, F.; Le Cerf, D. Analysis of arabic gum: Study of degradation and water desorption processes. *Food Hydrocoll*. **2009**, 23, 1930-1934.
52. Tiwari, A.; Terada, D.; Kobayash. Polyvinyl modified guar-gum bioplastics for packaging applications. Handbook of Bioplastics and Biocomposites Engineering Applications. **2011**, 24, 177.
53. Nakashima, T.; Xu, C.; Bin, Y.; Matsuo, M. Morphology and mechanical properties of poly (vinyl alcohol) and starch blends prepared by gelation/crystallization from solutions. *Colloid. Polym. Sci*. **2001**, 279, 646-654.
54. Huang, X.; Netravali, A. Biodegradable green composites made using bamboo micro/nano-fibrils and chemically modified soy protein resin. *Compos. Sci. Technol*. **2009**, 69, 1009-1015.
55. Padil, V.V.T.; Nguyen, N.H.; Ševců, A.; Černík, M. Fabrication, characterization, and antibacterial properties of electrospun membrane composed of gum karaya, polyvinyl alcohol, and silver nanoparticles. *J. Nanomater*. **2015[a]**, 271, 32-38.
56. Padil, V.V.T.; Cernik, M.; Tanger. Tree gum based electrospun nanofibre sheets: process optimization, characterization and environmental application. Nanocon 2014, 6th International Conference, Proceedings. **2015[b].**
57. Hindi, S.S.; Albureikan, M.O.I. System, apparatus, and methods for manufacturing biodegradable biopolymeric materials. US patent no. 11548192, Issue date: 01, 10, **2023**.
58. Volova, T.G;, Boyandin, A.N.; Vasil'ev, A.D.; Karpov, V.A.; Kozhevnikov, I.V.; Prudnikova, S.V.,; Gitel'Zon, I.I. Biodegradation of polyhydroxyalkanoates (PHAs) in the South China Sea and identification of PHA-degrading bacteria. *Microbiol*. **2011**, 80, 252.
59. Chen, J.; Zhang, Y.; Du, G. C.; Hua, Z. Z.; Zhu, Y. Biodegradation of polyvinyl alcohol by a mixed microbial culture. *Enzyme Microb. Technol*. **2007**, 40, 1686-1691.
60. Corti, A.; Solaro, R.; Chiellini, E. Biodegradation of poly (vinyl alcohol) in selected mixed microbial culture and relevant culture filtrate. ***Polym. Degrad. Stab.*** **2002**, 75, 447-458.
61. Rong, D.; Usui, K.; Morohoshi, T., et al. Symbiotic degradation of polyvinyl alcohol by *Novosphingobium* sp. and *Xanthobacter flavus*. *J.* ***Environ. Biotechnol.*** **2009**, 9, 131-134.

62. Abd Alla, F.A.A. The Effects of microbiological biodegradation on gum Arabic structure and molecular mass. PhD dissertation, Sudan University of Science and Technology. **2012**.
63. Wail, F.; Sabir, A.; Jacob, K. I. Novel reverse osmosis membranes composed of modified PVA/gum Arabic conjugates: Biofouling mitigation and chlorine resistance enhancement. *Carbohydr. Polym.* **2017**, 155, 28-39.
64. Solomon, M.M., et al. Gum Arabic-silver nanoparticles composite as a green anticorrosive formulation for steel corrosion in strong acid media. *Carbohydr. Polym*. **2018**, 181, 43-55.
65. Tahsiri, Z. et al. Gum Arabic improves the mechanical properties of wild almond protein film. *Carbohydr. Polym*. **2019**, 114994.
66. Ling, M. et al. Dual-functional gum Arabic binder for silicon anodes in lithium ion batteries. *Nano Energy*. **2015**, 12, 178-185.
67. Silvestri, D.; Mikšíček, J.; Wacławek, S.; Torres-Mendieta; R., Padil, V.V.; Černík, M. Production of electrospun nanofibers based on graphene oxide/gum Arabic. *Int. J. Biol. Macromol.* **2019**, 124, 396-402.
68. Lubambo, A.F.; de Freitas, R.A.; Sierakowski, M.R.; Lucyszyn, N.; Sassaki, G.L.; Serafim, B. M.; Saul, C. K. Electrospinning of commercial guar-gum: Effects of purification and filtration. *Carbohydr. Polym*. **2013**, *93*, 484-491.
69. Tieguhong, J.C.; Ndoye, O. Development of trade and marketing of non-wood forest products for poverty alleviation Africa. Paper presented at the workshop on lessons learnt on SFM in Africa. Uppsala, Sweden. 18-22 October, 2004.
70. Anonymous[c]. Policy note: export marketing of gum arabic from Sudan. Washington, D.C. World Bank Group. Available online: http://documents.worldbank.org/curated/en/736741468334873447/Policy-note-export-marketing-of-gum-arabic-from-Sudan (accessed on 02 March 2023).
71. ElKhawad , H.; ElBagher, M.A. Gum Arabic processing and marketing in the Sudan. MSc Thesis in Chemical Engineering, Khartoum, Sudan. **2008**.
72. Naili, D. and Wenzhi, D. Technology for producing gum Arabic powder. Chinese patent, application no. CN 101143995A, Publication date: 03-19-**2008**.
73. Chikamai, B.N.; Banks, W.B.; Anderson, D.M.W.; Weiping, W. Processing of gum Arabic and some new opportunities. *Food Hydrocoll*. 1996, 10, 309-316.
74. Schmidt, M.W.; Torn, M.S.; Abiven, S.; Dittmar, T.; Guggenberger, G.; Janssens, I.A.; Trumbore, S. E. Persistence of soil organic matter as an ecosystem property. *Nature*. **2011**, 478, 49-56.
75. Abdalla, I.G.E. Enzymatic degradation and analysis of gum Arabic. PhD thesis, UOFK. **2015.**
76. Freedman, Z.; Zak, D.R. Soil bacterial communities are shaped by temporal and environmental filtering: evidence from a long-term chronosequence. *Environ. Microbiol.* **2015**, 17, 3208–3218.
77. Turner, S.; Mikutta, R.; Meyer-Stüve, S.; Guggenberger, G.; Schaarschmidt, F.; Lazar, C. S.; Schippers, A. Microbial community dynamics in soil depth profiles over 120,000 years of ecosystem development. *Front. Microbiol*. **2017**, 8, 874.
78. Adam, F.A.; Abdellah, A.M.; Abdel-Magid, H.M.; Osman, M.E.; Al-Aassaf S.; Phillips, G.O. Effect of some isolated bacterial species on the physicochemical aspects and main components of gum arabic (*Acacia senega*l var. *senegal*). Int. J. Dev. Res. **2018**, 8, 18436-18442.
79. Wu, H.F.; Yue, L.Z.; Jiang, S.L.; Lu, Y.Q.; Wu, Y.X.; Wan, Z.Y. Biodegradation of polyvinyl alcohol by different dominant degrading bacterial strains in a baffled anaerobic bioreactor. *Int. J. Dev. Res*. **2019**, 79, 2005-2012.
80. Ibrahim, M.; Krejčík, M.; Havlíček, K.; Petrík, S.; Eldessouki, M. Evaluation of chemical and physical properties of biodegradable gum Arabic/PVA/Ag nanofibrous membranes as a potential wrapping material. *J. Eng. Fibers Fabr*. **2020**, *15*, 1558925020946451.
81. Hao, J.; Chai, Y.N.; Lopes, L.D.; Ordóñez, R.A.; Wright, E.E.; Archontoulis, S.; Schachtman, D.P. The effects of soil depth on the structure of microbial communities in agricultural soils in Iowa, USA. *Appl Environ Microbiol*. **2021**, 87, e02673-20.
82. Sichert, A.; Cordero, O.X. Polysaccharide-bacteria interactions from the lens of evolutionary ecology. *Front Microbiol*. **2021**, 12, 705082.
83. Polman, E.M.; Gruter, G. J. M.; Parsons, J. R.; Tietema, A. Comparison of the aerobic biodegradation of biopolymers and the corresponding bioplastics: A review. *Science of the Total Environment*. **2021**, *753*, 141953.
84. Villa-Rivera, M.G.; Cano-Camacho, H.; López-Romero, E.; Zavala-Páramo, M.G. The role of arabinogalactan type II degradation in plant-microbe interactions. *Frontiers in microbiology*. **2021**, 12, 730543.
85. Sasaki, Y.; Uchimura, Y.; Kitahara, K.; Fujita, K. Characterization of a GH36 α-D-galactosidase associated with assimilation of gum Arabic in *Bifidobacterium longum* subsp. longum JCM7052. *J. of appl. glycosci*. **2021**, 68, 47-52.
86. Chien, H.-L.; Tsai, Y.-T.; Tseng, W.-S.; Wu, J.-A.; Kuo, S.-L.; Chang, S.-L.; Huang, S.-J.; Liu, C.-T. Biodegradation of PBSA films by *Elite Aspergillus* isolates and farmland soil. *Polym*. **2022,** 14, 1320.
87. Sasaki, Y.; Komeno, M.; Ishiwata, A.; Horigome, A.; Odamaki, T.; Xiao, J. Z.; Fujita, K. Mechanism of cooperative degradation of gum arabic arabinogalactan protein by *bifidobacterium longum* surface enzymes. *Appl Environ Microbiol*. **2022**, 88, e02187-21.
88. Santos-Beneit, F.; Chen, L.M.; Bordel, S.; Frutos de la Flor, R.; García-Depraect, O.; Lebrero, R.; Rodriguez-Vega, S.; Muñoz, R.; Börner, R.A.; Börner, T. Screening enzymes that can depolymerize commercial biodegradable polymers: Heterologous expression of *Fusarium solani* cutinase in *Escherichia coli*. *Microorganisms*. **2023**; 11:328.
89. Tang, Y.; Zhou, D.; Zhang, J. Novel polyvinyl alcohol/styrene butadiene rubber latex/carboxymethyl cellulose nanocomposites reinforced with modified halloysite nanotubes. *J. Nanomater*. **2013**, 2013: 1-8.
90. Chiellini, E.; Corti, A.; Solaro, R. Biodegradation of poly (vinyl alcohol) based blown films under different environmental conditions. ***Polym. Degrad. Stab.*** **1999**, 64, 305-312.
91. Jayasekara, R.; Harding, I.; Bowater, I.; Christie, G.B.; Lonergan, G.T. Biodegradation by composting of surface modified starch and PVA blended films. *J. Polym. Environ*. **2003**, 11, 49-56.

92. Matsumura, S.; Tanaka, T. Novel malonate-type copolymers containing vinyl alcohol blocks as biodegradable segments and their builder performance in detergent formulations. *J. Appl. Polym. Sci*. **1994**, 2, 89-97.
93. Hindi, S.S.; Albureikan, M.Othman.I.; Al-ghamdy, A.A.; Alhummiany, H.; Ansari, M.S. Synthesis and characterization of gum Arabic based bioplastic membranes. *J. Nanosci. Nanotechnol. Res.* **2017**[a], 4, 32-42.
94. Hindi, S.S.; Albureikan, M.O.I.; Attieh A. Al-ghamdy, A.A.; Alhummiany, H.; Al-Sharabi, S.M. Effect of potassium dichromate on properties and biodegradation of gum Arabic based bioplastic membranes. *Nanosci. Nanotechnol. Res*. **2017**[b], 4, 49-58.
95. Hindi, S.S. Some crystallographic properties of cellulose I as affected by cellulosic resource, smoothing, and computation methods. *Int. J. Innov. Res. Sci*. **2017**[a], 6, 732-752.
96. Hindi, S.S. Suitability of date palm leaflets for sulphated cellulose nanocrystals synthesis. *J. Nanosci. Nanotechnol. Res*. **2017**[b], 4, 7-16.
97. Hindi, S.S. 2017[e]. Nanocrystalline cellulose: Synthesis from pruning waste of *Zizyphus spina christi* and characterization. *J. Nanosci. Nanotechnol*. **2017**[c], 4:106-114.
98. Fortunati, E.; Puglia, D.; Monti, M.; Peponi, L.; Santulli, C.; Kenny, J.M.; Torre, L. Extraction of cellulose nanocrystals from *Phormium tenax* fibres. *J. Polym. Environ*. **2013**, 21, 319-328.
99. Al-Solaimani, S.G. Chemical properties of soils and underground water of Hada Al-Sham Research Station, Kingdom of Saudi Arabia. *J. Environ. Sci*. Ain Shams University. **2003**[a], 6, 257-284.
100. Al-Solaimani, S.G.; Al-Toukhy, A.; Al-Zahrani, S. Mineral characteristics, classification and evaluation of soils of Hada Al-Sham Res. Station, Kingdom of Saudi Arabia. *J. Environ. Sci.*, Ain Shams University. **2003**[b]. 6, 285- 322.
101. Mostafa, H.M.; Sourell, H.; Bockisch, F.J. Mechanical properties of some bioplastics under different soil types used as biodegradable drip tubes. *Agric. Eng. Int.: CIGR J*. **2010**, 12, 12-21.
102. El-Nakhlawy, F.S. Principles of statistics, biostatistical experimental design and analysis. KAU Pub. Center. KSA. **2008**.
103. Sismanoglu, T. et al. Preparation and characterization of antibacterial Senegalia (acacia) Senegal / iron - silica bio-nanocomposites, *Appl. Surf. Sci*. **2015**. 354, 250-255.
104. Bouaziz, F.; Koubaa, M.; Barba, F.J.; Roohinejad, S.; Chaabouni, S.E. Antioxidant properties of water-soluble gum from flaxseed hulls. *Antioxidants*. **2016**, *5*, 26.
105. Anicuta, S.-G.; Dobre, L.; Stroescu, M.; Jipa, I. Fourier transform infrared (FTIR) spectroscopy for characterization of antimicrobial films containing chitosan. Analele UniversităŃii din Oradea Fascicula: Ecotoxicologie, Zootehnie si Tehnologii de Industrie Alimentară. **2010**, 1234-1240.
106. Rathna, G.V.N.; Jog, J. P.; Gaikwad, A.B. Development of non-woven nanofibers of egg albumen-poly (vinyl alcohol) blends: influence of solution properties on morphology of nanofibers. *Polym. J*. **2011**, 43, 654-661.
107. Mori, T.; Sakimoto, M.; Kagi, T.; Sakai, T. Isolation and characterization of a stra108-in of Bacillus megaterium that degrades poly (vinyl alcohol). *Biosci. Biotechnol. Biochem*. **1996**, 60, 330-332.
108. Patil, R.; Bagde, U.S. Enrichment and isolation of microbial strains degrading bioplastic polyvinyl alcohol and time course study of their degradation potential. *African J. Biotechnol*. **2015**, 14, 2216-2226.
109. Jecu, L.; Gheorghe, A.; Rosu, A.; Raut, I.; Grosu, E.; Ghiurea, Marius. Ability of fungal strains to degrade PVA based materials. *J Polym Environ*. **2010**, 18. 284-290.
110. Kawai, F.; Hu, X. Biochemistry of microbial polyvinyl alcohol degradation. *Appl. Microbiol. Biotechnol*. **2009**. 84, 227-237.
111. Cadmus, M.C.; Jackson, L.K.; Burton, K.A.; Plattner, R.D.,; Slodki, M.E. Biodegradation of xanthan gum by Bacillus sp. *Appl. Environ. Microbiol*. **1982**, 44, 5-11.
112. Busoloa, T.; Urab, D.P.; Kima, S.K.; Marzecc, M.M.; Bernasik, A.; Stachewicz, U.; Kar-Narayan, S. Surface potential tailoring of PMMA fibers by electrospinning for enhanced triboelectric performance. *Nano Energy*. **2019**, 57, 500–506.
113. Anonymous[d]. National Center for Biotechnology Information. PubChem Compound Summary for CID 11199, polyvinyl alcohol. Available online: https://pubchem.ncbi.nlm.nih.gov/compound/Vinyl-alcohol. **2023**. (accessed on March 11, 2023.
114. Anonymous[e]. National Center for Biotechnology Information. PubChem Substance Record for SID 50019090, 2-Methyl-2-propenoic acid methyl ester homopolymer, Source: LeadScope. **2023**. Available online: https://pubchem.ncbi.nlm.nih.gov/substance/50019090 (accessed on 12 March 2023).
115. Anonymous[f]. PubChem, compound summary for CID 24847856, Galactoarabinan; **2023**. Available online: https://pubchem.ncbi.nlm.nih.gov/compound/Galactoarabinan. (accessed on 08 March 2023).
116. Anonymous[g]. National Center for Biotechnology Information. PubChem, compound Summary for CID 439212, glycoprotein. **2023**. Available online: https://pubchem.ncbi.nlm.nih.gov/compound/Glycoprotein (accessed on 13 March 2023).
117. Anonymous[h]. National Center for Biotechnology Information. PubChem, substance record for SID 405234199, a plant arabinogalactan-[protein], Source: BioCyc. **2023**. Available online: https://pubchem.ncbi.nlm.nih.gov/substance/405234199. (accessed on 22 March 2023).
118. Schmidt, D.; Coburn, C.; DeKoven, B. et al. Water-based non-stick hydrophobic coatings. *Nature*. **1994**, 368, 39–41.
119. Hild, F. Surface energy of plastics. **2009**. Available online: https://www.tstar.com/blog/bid/33845/surface-energy-of-plastics (accessed on 22 March 2023).
120. Zi, Y.; Wang, Z.L. Nanogenerators: An emerging technology towards nanoenergy. **2017**, *APL Materials* 5, 074103
121. Randall, R.C.; Phillips, G.O.; Williams, P.A. The role of the proteinaceous component on the emulsifying properties of gum arabic. *Food hydrocoll*. **1988**, 2, 131-140.
122. Randall, R.C.; Phillips, G.O.; Williams, P.A. Fractionation and characterization of gum from *Acacia senegal*. *Food hydrocoll*. **1989**, 3, 65-75.

 doi:10.20944/preprints202305.1803.v1

123. Azzaoui, K.; Hammouti, B.; Lamhamdi, A.; Mejdoubi, E.; Berrabah, M. The gum Arabic in the southern region of Morocco. *Mor. J. Chem*. **2014**, 3, Mor-J.
124. Elsabee, M.Z.; Naguib, H. F.; Morsi, R.E. Chitosan based nanofibers, review. *Mater. Sci. Eng*. C. **2012**, 32, 1711-1726.
125. Pakravan, M.; Heuzey, M.C.; Ajji, A.A fundamental study of chitosan/PEO electrospinning. *Polym. J.* **2011**, 52, 4813-4824.
126. Wiśniewska, M.; Bogatyrov, V.; Ostolska, I.; Szewczuk-Karpisz, K.; Terpiłowski, K.; Nosal-Wiercińska, A. Impact of poly(vinyl alcohol) adsorption on the surface characteristics of mixed oxide Mn x O y –SiO_2 . *Adsorption*. **2016**, 22, 417–423.
127. Chibowski, S., Paszkiewicz, M., Krupa, M. Investigation of the influence of the polyvinyl alcohol adsorption on the electrical properties of Al_2O_3–solution interface, thickness of the adsorption layers of PVA. *Powder Technol*. **2000**, 107, 251-255.
128. Nuraje, N.; Khan, W.S.; Lei, Y.; Ceylan, M.; Asmatulu, R. Superhydrophobic electrospum nanofibers. *J. Mater. Chem. A.1*. **2013,** 1929-1946.
129. Osti, G.B.F.; Wolf, F.G.; Philippi, P.C. Spreading of liquid drops on acrylic surfaces. 20th International Congress of Mechanical Engineering. November 15-20, **2009**, Gramado, RS, Brazil.
130. Johnson, R.E., Dettre, R.H. Wetting of low-energy surfaces. Marcel Dekker: New York, **1993**.
131. Hild, F. Surface energy of plastics. **2023**. https://www.tstar.com/blog/bid/33845/surface-energy-of-plastics.
132. Ibekwe, C.A.; Oyatogun, G.M.; Esan, T.A.; Oluwasegun, K.M. Synthesis and characterization of chitosan/gum Arabic nanoparticles for bone regeneration. *Am. J. Mater. Sci. Eng*. **2017**, 5, 28-36.
133. Mir, M.B.; Haripriya, S. Assessment of physical and structural characteristics of almond gum. *Int. J. Biol. Macromol*. **2016**. 93, 476–482.
134. Stuart, B.H. Infrared spectroscopy: Fundamentals and applications, first ed., John Wiley & Sons Ltd, West Sussex, **2004**.
135. Kumar, A.; Negi, Y.S.; Choudhary, V.; Bhardwaj, N.K. Characterization of cellulose nanocrystals produced by acid-hydrolysis from sugarcane bagasse as agro-waste. *Mater. Chem. Phys*. **2014**, 2, 1-8.
136. Yoshimi, Y., Yaguchi, K., Kaneko, S., Tsumuraya, Y., and Kotake, T. Properties of two fungal endo-beta-1,3-galactanases and their synergistic action with an exo-beta-1,3-galactanase in degrading arabinogalactan-proteins. *Carbohydr. Res.* **2017**, 45, 26–35.
137. Yoshimi, Y., Hara, K., Yoshimura, M., Tanaka, N., Higaki, T., Tsumuraya, Y., et al. Expression of a fungal exo-beta-1,3-galactanase in *Arabidopsis* reveals a role of type II arabinogalactans in the regulation of cell shape. *J. Exp. Bot.* **2020,** 71, 5414–5424.